hydrology

MDPI

Article

Performance Evaluation of a Distributed Hydrological Model Using Satellite Data over the Lake Kastoria Catchment, Greece

Dimitris Papadimos [1,*] and Dimitris Papamichail [2]

[1] The National Museum of Natural History Goulandris—Greek Biotope/Wetland Centre, GR 57001 Thessaloniki, Greece
[2] Department of Hydraulics, Soil Science and Agricultural Engineering, Faculty of Agriculture, Forestry and Natural Environment, Aristotle University of Thessaloniki, GR 54124 Thessaloniki, Greece; papamich@agro.auth.gr
* Correspondence: papadimos@ekby.gr; Tel.: +30-2310-473320

Abstract

It might be difficult in many countries to find extended time series of measurements related to parameters of lakes' hydrology and their interactions with catchments. Nowadays, the combined use of satellite imagery and spatially distributed hydrological models may contribute substantially to this direction. In this study, in order to assess for a long period of years a lake's surface elevation (LSE) and its water balance components, Lake Kastoria and its catchment, under Greece's dry-thermal conditions, were selected as the case study. This research employed the MIKE SHE coupled with the MIKE HYDRO River (MHR) hydrological modeling system, fed with precipitation and leaf area index (LAI) data coming from a ground weather station, typical values of LAI for the specific area, and satellite products from NASA for the precipitation and from Copernicus Global Land Service for the LAI. In all cases where satellite data were used, the simulation of the long-term LSE was very satisfactory, with minor to medium changes to the inflow and outflow components of the water balance in both the catchment (from 0.32 to 7.36%) and the lake (from 1.47 to 11.3%). The above changes were also reflected in the runoff coefficients. In conclusion, the above satellite products can adequately be used for the prediction of the LSE. Furthermore, a plethora of quantified information in relation to the catchment's water balance can be extracted and used in decision-making processes.

Keywords: Kastoria Lake; spatially distributed hydrological modeling; MIKE SHE; MIKE HYDRO River; satellite precipitation; GPM_3IMERGDF; satellite LAI; GEOV3

Check for updates

Academic Editor: Changsen Zhao

Received: 3 November 2025
Revised: 16 December 2025
Accepted: 17 December 2025
Published: 20 December 2025

Copyright: © 2025 by the authors. Licensee MDPI, Basel, Switzerland. This article is an open access article distributed under the terms and conditions of the Creative Commons Attribution (CC BY) license.

1. Introduction

The development and use of spatially distributed hydrological models have been well established for several decades, e.g., MIKE SHE [1–3], HSPF [4], SWAT [5], HEC-HMS [6], AnnAGNPS [7], ANSWERS-Continuous [8], and VIC [9]. Among the above, MIKE SHE is considered one of the most integrated physically based hydrological models. It has been used in a variety of applications worldwide [10–13] and in Greek conditions [14–18].

The great demand for spatially distributed data of the above models limits their use or even makes them unselected in many areas of interest. During the last decades, the development of global-scale (or even at continent scale) geospatial datasets related, e.g., to terrain models (STRM data [19]), land use (CORINE Land Cover [20,21]), or soil types (ESDB-ESDAC [22,23]), has come to facilitate their application by providing data in un-

gauged catchments. However, the availability of spatio-temporal data such as precipitation height and Leaf Area Index (LAI) still remains very low.

In Greece, the spatial coverage with ground-based precipitation observation stations remains insufficient, with an even greater problem in mountainous areas. Meeting the needs for precipitation data for the application of spatially distributed hydrological models is often assisted by using neighboring catchment precipitation stations or rainfall lapse rates from research work of past years or decades, which affects the accuracy of the model's results.

Regarding LAI, its assessment in Greece has been sporadic, carried out in the field using conventional methods (e.g., destructive sampling), and focused on specific forest species or forest areas [24] and mainly on agricultural crops [25–27]. Although these methods are considered more accurate, they involve time-consuming, laborious, and costly procedures [28,29]. Nowadays, the almost widespread adoption of the use of hydrological models in the field of water resource management has led to the use of satellite LAI data with satisfactory spatial and temporal resolution [30].

Satellite precipitation and LAI products are continuously developing alternative sources of spatio-temporal hydrological information. In regard to precipitation, in recent years, several satellite products have been produced on a global scale, with high spatial and temporal resolution "https://disc.gsfc.nasa.gov/datasets?keywords=daily%25-20Rainfall&page=1 (accessed on 14 February 2023)"). They are available in near real-time and at zero cost [31], and their geographical coverage is uniform, including even hard-to-reach areas [32,33]. These characteristics make them suitable even for large-scale hydrological simulations, e.g., at the country level [34]. A similar development at the global level is also observed in the case of LAI [35,36]. Large organizations (e.g., FAO, ESA, and NASA) create and make available satellite-based LAI imaging products on a global scale and with a temporal resolution of even a few days.

To date, the use of satellite precipitation data in hydrological simulations has been investigated by a large number of researchers [37–42]. In Greece [43], precipitation with a time step of 3 h from the TRM satellite product was used to simulate flood events in the Pinios basin in the Peloponnese. Ref. [44] also investigated the possibility of using them to simulate flood events in catchments where precipitation data are not available. The above researchers have mainly focused on short-duration precipitation events (from a few hours to a few days) and the simulation of the resulting runoff or flood events.

Several researchers have investigated both surface water and groundwater of the Lake Kastoria catchment by using different modeling systems and time steps. However, Lake Kastoria is not included in their models as a water body. Instead, it is approached as a boundary condition with a predefined surface elevation [45,46]. Furthermore, hydrology in its catchment is always investigated in a fragmented way (e.g., firstly rainfall–runoff in the mountainous part, then in the lowland, and finally the groundwater dynamics) and not in an integrated way, due to the restricted capabilities of the modeling systems that have been used.

In this study, we investigate the ability of using long-term satellite precipitation and LAI data, in combination with an integrated surface water—groundwater and fully distributed modeling system—the MIKE SHE/MIKE HYDRO River—to simulate the hydrological regime and surface elevation of Lake Kastoria in Northern Greece. MHR [47–49], which is the successor of MIKE 11 [49,50], simulates one-dimensional water flow in rivers and lakes and is here coupled with MIKE SHE to fully simulate their interaction with overland water and the saturated zone in the catchment.

The model was setup in the entire catchment area of the lake, calibrated and validated for the period November 2012–December 2022 against monthly surface elevation measurements of Lake Kastoria, through an extended sensitivity analysis, by using precipitation data from a local available weather station and typical values of LAI in North Greece.

Subsequently, satellite precipitation and LAI data were used in the calibrated model, and the results were compared to the previous ones.

The satellite precipitation product that was used was the GPM Level 3 IMERG Final Daily 10 × 10 km, V06 (GPM_3IMERGDF) https://disc.gsfc.nasa.gov/dtasets/GPM_3IMERGDF_06/summary (accessed on 14 February 2023, now replaced by V07 at "https://disc.gsfc.nasa.gov/datasets/GPM_3IMERGDL_07/summary?keywords=imerg, accessed on 14 February 2023). Two other products with fine spatial resolution are CHIRPS and PDIR-NOW. CHIRPS (Climate Hazards InfraRed Precipitation with Station data—"https://climatedataguide.ucar.edu/climate-data/chirps-climate-hazards-infrared-precipitation-station-data-version-3 (accessed on 14 February 2023)" has a finer spatial resolution (0.05° × 0.05°); however, it does not directly provide daily estimates of precipitation (they are downscaled from pentadal (5-day) estimates). PDIR-NOW (PERSIANN Dynamic Infrared–Rain Rate—"https://chrsdata.eng.uci.edu/ (accessed on 14 February 2023)" also has a finer spatial resolution (0.04° × 0.04°); however, this product was formally launched in 2020, during the course of this research. The satellite product used for LAI was the VPROVA-V LAI, 300 m Version 1.0 (GEOV3). Both products were selected due to their availability for the period of interest, 2012–2022, and their high spatial resolution in comparison to the competition.

2. Materials and Methods

2.1. Study Area

The study area is located in Northwest Greece and includes Lake Kastoria and its catchment (Figure 1). It extends over 262.72 km^2 and is bordered by mountain ranges. The elevation in the catchment varies from 595 to 700 m above mean sea level (a.m.s.l.) at the lowlands, up to 2049 m at its highest peak. The mean annual rainfall during the study period (November 2012–December 2022) has been estimated to be 713 mm, while the mean monthly temperature ranges from −1 °C during winter to 20 °C in summer.

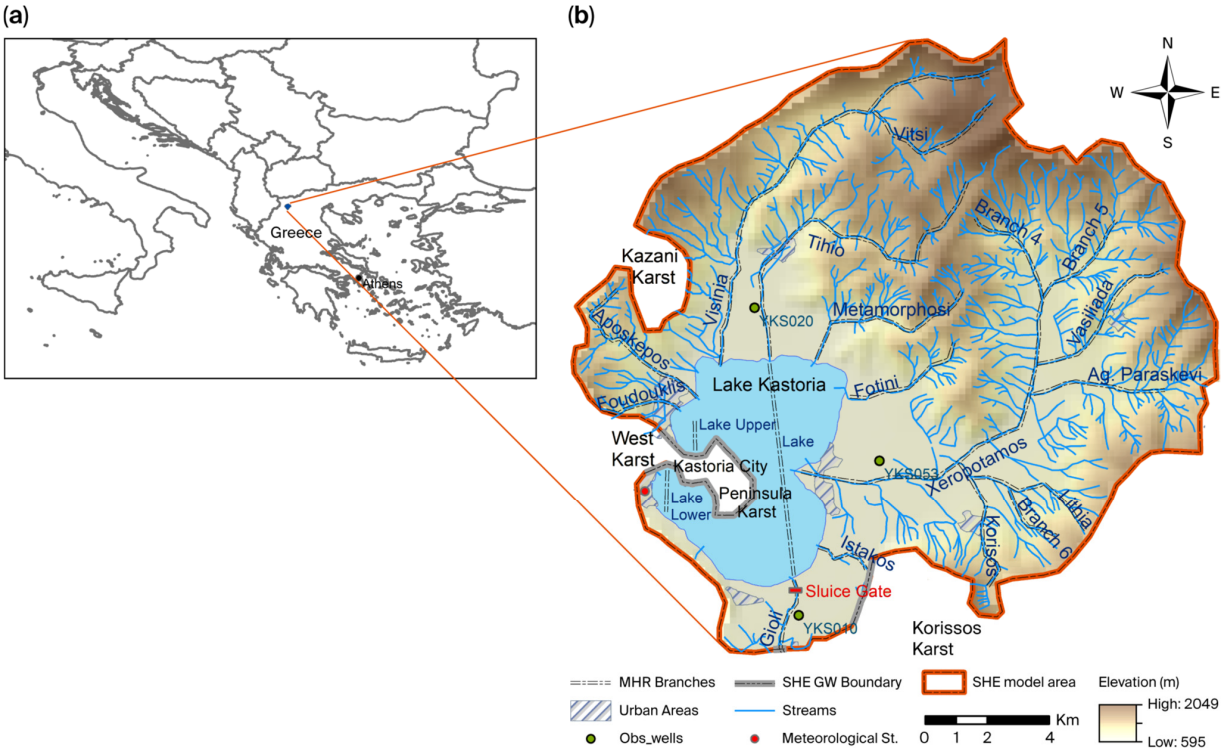


Figure 1. (**a**) position and (**b**) study site of Lake Kastoria catchment.

Lake Kastoria is fed with both surface water and groundwater. Surface water comes from the eight main streams, which drain its catchment, while groundwater comes from karstic springs located mainly in its western part (Peninsula and western karstic formations). The lake's water level (WL) is being adjusted by a sluice gate, which is located at the beginning of the Gioli stream where the lake outflows. The maximum discharge through the gate is 3.33 m^3/s when the lake surface elevation (LSE) is at 627.45 m a.m.s.l. During the study period, the LSE fluctuated between LSE_{min} = 626.4 m and LSE_{max} = 627.30 m a.m.s.l., while the lake's volume and surface area ranged from $V_{min} = 96.46 \times 10^6$ m^3 and A_{min} = 28.57 km^2 to $V_{max} = 123 \times 10^6$ m^3 and A_{max} = 31.75 km^2 for the aforementioned LSE. The mean maximum depth of the lake varies between 7.0 and 8.0 m.

The main water user in the catchment is irrigated agriculture. About 3200 ha are irrigated using groundwater and subsequently surface water from the lake and the streams. The prevailing crops are apple orchards, beans, vegetables, maize, and fodder plants.

Kastoria is the main urban complex in the catchment and is located on the western shores of the lake. Its population is about 23,500 residents. However, most of its water supply needs are covered by sources that are located outside of the catchment.

2.2. Data Collection

Daily data of precipitation and temperature were obtained from the meteorological station of Kastoria (Unit METEO of the National Observatory of Athens, "https://www.meteo.gr/ (accessed on 14 February 2023)"). For the estimation of the lapse rates of the above parameters and their spatial distribution in the catchment, mean monthly data were acquired and used from the climatic atlas "http://climatlas.hnms.gr/ (accessed on 10 April 2019)" of the Hellenic National Meteorological Service (HNMS).

The Digital Terrain Model (DTM) of the catchment was obtained from the SRTM data [19] with a spatial resolution of 90 m. Data related to hydrogeology were retrieved from [51–53]. Regarding the water table near the lake, data were acquired from the National Monitoring Water Network for Water Framework Directive (WFD) "http://nmwn.ypeka.gr/?q=groundwater-stations (accessed on 14 February 2023)". They refer to measurements at three observation wells close to the lake (ΥKS020, ΥKS053, and ΥKS010), to its north, east, and west shores (Figure 1). Also, piezometric data in the plain part of the catchment were acquired by [51]. The soil types and their spatial distribution (Figure 2) were extracted from the ESDB—ESDAC [22,23]. The water retention characteristics for each of the above soil types were acquired from [54] and [17]. Data related to land uses were downloaded from the Corine Land Cover database for the years 2012 and 2018 [20,21]. Since no changes were observed in the two datasets, neither in their classes nor in the size of their polygons, finally, the pattern from [21] was adopted (Figure 2).

2.2.1. Satellite Precipitation Data

Daily data of satellite precipitation measurements were obtained from the mission of Global Precipitation Measurement—GPM [55] and its product GPM Level 3 IMERG Final Daily 10 × 10 km, V06 (GPM_3IMERGDF) [56]. The latter is produced from the primary product GPM_3IMERGHH of the mission—it includes precipitation measurements every half hour—by simple summation of its 24 h observations "https://disc.gsfc.nasa.gov/datasets/GPM-3IMERGDF_06/summary (accessed on 14 February 2023, now replaced by V07 at "https://disc.gsfc.nasa.gov/datasets/GPM_3IMERGDL_07/summary?keywords=imerg)". Using the IMERG-Final product rather than IMERG-Early or IMERG-Late is also recommended—due to its improved accuracy and post-processing corrections—for scientific research where timeliness is not a requirement "https://gpm.nasa.gov/data/directory (accessed on 14 February 2023)". The datasets of the GPM_3IMERGDF product

are provided in NETCDF file format (one file for each day of the year). The total number of files downloaded from the NASA server was 3347 files for the period from 1 November 2012 to 31 December 2022.

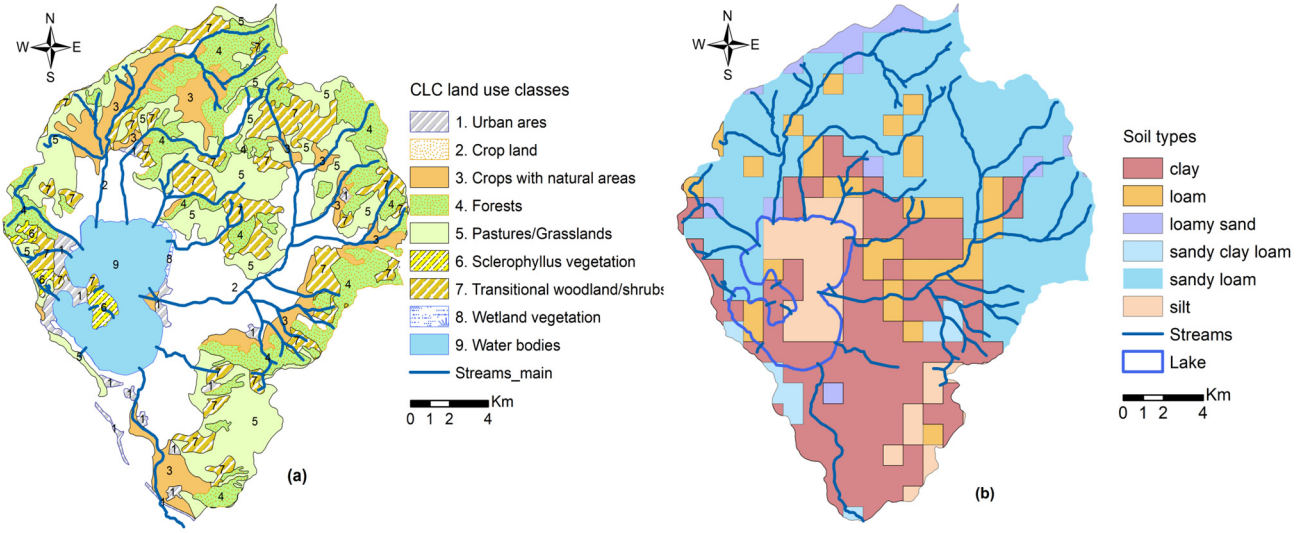


Figure 2. (**a**) Aggregated land use classes extracted from Corine Land Cover and (**b**) soil types in the Lake Kastoria catchment.

2.2.2. Satellite LAI Data

The PROVA-VLAI300m V1.0 (GEOV3) product of the CGLS (Copernicus Global Land Service) "https://land.copernicus.eu/global/products/lai (accessed on 14 February 2023)" was utilized. Its spatial resolution ranks among the highest available, at approximately 300 m × 300 m, which is comparable to the discretization scale adopted in the MIKE SHE hydrological model (200 m × 200 m). The temporal resolution of the dataset is 10 days. A detailed description of the technical specifications of the GEOV3 product can be found in the user manual provided by [57]

The LAI data were obtained in *.tiff file format (one file representing a ten-day period). The total number of available files, which were downloaded from the CGLS server, was 149 files and covered the period from 20 August 2014 to 31 December 2019, with gaps between them. From the above period, mean values of LAI for each ten-day period for each month were estimated for each Corine Land Cover (CLC) category in the catchment.

2.3. The Modeling Systems MIKE SHE and MIKE HYDO River (MHR)

The coupled MIKE SHE/MHR modeling systems have been used for the purposes of this study. MIKE SHE is a fully distributed hydrological simulation system, able to simulate almost all the main components of the hydrological cycle, and is dynamically coupled with MHR. MHR is a deterministic one-dimensional, finite-difference system, which simulates the flow of water in open conduits (e.g., rivers, deltas, lakes, etc.), hydraulic structures (e.g., spillways, gates, etc.), as well as water management practices. It is called by MIKE SHE at each time step, allowing for the accurate simulation of the interactions between the water flowing into rivers and lakes, overland water, and groundwater.

The model components of MIKE SHE/MHR, the simulated processes, the coupling, the governing equations, and the dimensions of the solution scheme that have been used in this research are given in Table 1 [58,59].

Table 1. MIKE SHE (SHE) and MIKE HYDRO River (MHR) components, simulated processes of the hydrological cycle, coupling, governing equations, and dimensions of the solution schemes that have been used in the hydrological model of the Lake Kastoria catchment.

Model Component	Simulates	Fully Dynamic Coupling	Dimension	Governing Equation
SHE, OL *	Overland sheet flow and water depth, Depression storage	SHE SZ, UZ & MHR	2D	Saint–Venant's (Kinematic wave approximation)
MHR	River hydraulics (flow and water level)	SHE SZ, OL	1D	Saint-Venant's equation (Fully dynamic wave approximation)
SHE, UZ *	Flow and water content of the unsaturated zone, infiltration, and groundwater recharge	SHE SZ, OL	1D	Richard's equation
SHE SF *	Snowmelt and freezing	SHE UZ	-	Degree-day method
SHE ET *	Soil and free water surface evaporation, plant transpiration	SHE UZ, OL	-	Kristensen and Jensen
SHE SZ *	Saturated zone (groundwater) flows and water levels	SHE UZ, OL & MHR	3D	Boussinesq's equation
SHE IR *	Irrigation demands (soil water deficit) and allocation (surface water/ground water)	SHE SZ & MHR	-	-

* OL (Overland Flow), ET (Evapotranspiration), SZ (Saturated Zone), IR (Irrigation), UZ (Unsaturated Zone), and SF (Snowmelt and Freezing).

2.4. MIKE SHE Model Setup

The model domain includes the whole catchment of the lake excluding the karstic formations (Figure 1). It has been discretized with a cell size of 200 m × 200 m (130 rows × 120 columns). This size assures a reasonable computational time for the 10-year simulation period with a maximum time step of 1 h and the accuracy with which the physiographic features of the basin (lake, rivers, land uses, soils, etc.) and the associated results are spatially represented.

The DTM of the catchment was further enhanced with the bathymetry of the lake [60] and finally resized to the cell size.

The spatial distribution of both daily precipitation and evapotranspiration in the model domain was carried out on the basis of hypsometric zones where the above parameters are considered uniform. The catchment was divided into 8 hypsometric zones. The first one is extended from 600 to 700 m a.m.s.l., while each subsequent zone occupies areas up to 200 m higher, until the altitude of 2100 m a.m.s.l. The daily values of precipitation and temperature in each zone were calculated taking into account the daily data from the Kastoria station, the mean elevation in the zone, and the lapse rates of the above parameters in the catchment. Daily time series of reference evapotranspiration (ET_o, mm/day) were calculated following [61–63] and by adopting the adjustment for the Greek climatic conditions, proposed by [64]. The calculations were conducted for each hypsometric zone using the associated temperature values.

When satellite precipitation data were used, the spatial distribution of GPM_3IMERGDF precipitation was adapted in the MIKE SHE model as follows. A NetCDF-4 file of the product was first converted into a grid file. Next, the centers of the resulting grid cells (data points) were extracted to generate Thiessen polygons in a shapefile, representing the spatial-rainfall distribution over the catchment. This shapefile was then imported into the MIKE SHE model, and the rainfall time series for each polygon was extracted directly from

the corresponding GPM_3IMERGDF data points and assigned as precipitation input to the model.

Snowmelt and freezing were simulated following a modified degree-day method [58], in which the rate of melting increases as the air temperature increases. The lapse rate of the temperature in the catchment (−0.6 °C/100 m) was used for its spatial distribution. The required parameters from the method and their finally selected values were: (i) melting coefficient for thermal energy in rain (0.5/°C), (ii) melting temperature (0.0 °C), (iii) degree-day coefficient (2.5 mm/°C/d), (iv) minimum snow storage (0.0 mm), (v) max wet snow fraction (0.1), (vi) initial total snow storage (0.0 mm), and (vii) initial wet snow fraction (0). Although snowfall in the catchment is common during the winter, the depth and the duration of the snow cover do not significantly affect the catchment's hydrology. Therefore, no particular emphasis is placed on this process.

A total of 18 land use classes, following [21], were incorporated into the model. Their polygons were further cross-checked and adjusted following recent images from Google Earth and data related to the irrigated area in the catchment. For each land use class, further information was included in the model as follows:

- Temporal distribution of typical values for northern Greece of LAI and RD (Root Depth) during the year [65]. This distribution was kept the same for each subsequent year.
- Initial values for the parameters C_1 = 0.3, C_2 = 0.1, C_3 = 20 mm/day, C_{int} = 0.05, and AROOT = 1 for non-irrigated and AROOT = 1.5 for irrigated classes, of the [66] method for the calculation of evapotranspiration (ET). These parameters were subject to sensitivity analysis.
- Values for the crop coefficient K_c. For non-irrigated classes, K_c was set equal to one throughout the whole year, while for irrigated classes and the lake, K_c values were estimated following [63] and are shown in Figure 3.

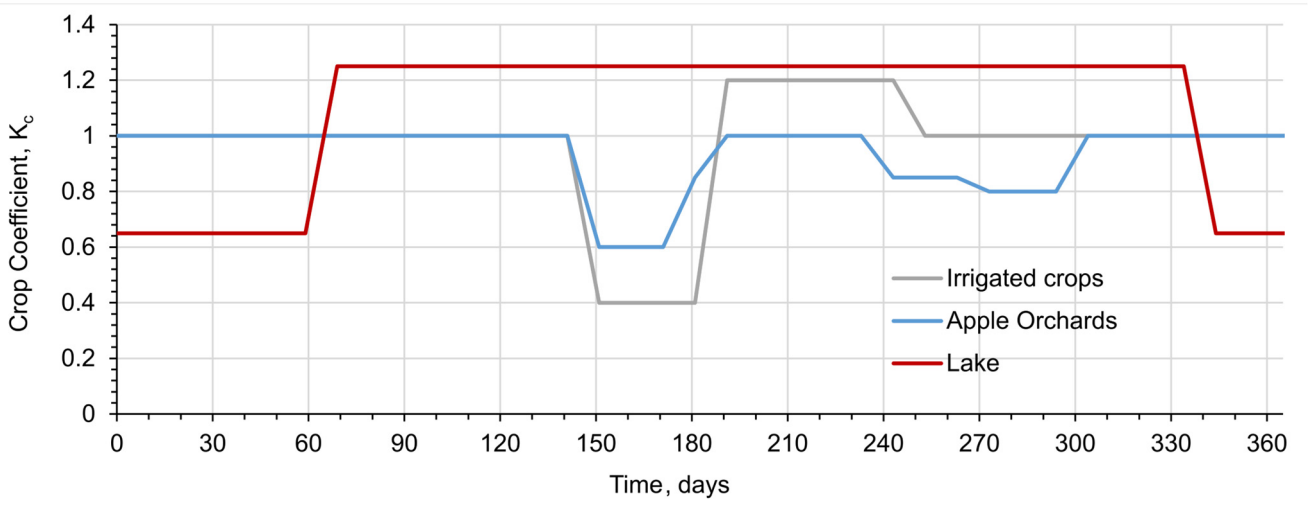


Figure 3. Temporal distribution of crop coefficients (K_c) for irrigated crops, apple orchards, and Lake Kastoria in the model of the Lake Kastoria catchment.

Irrigation needs for each cell (in irrigated land use classes), as well as irrigation start and stop, were set to be carried out by the MIKE SHE environment, based on a predefined irrigation period and soil moisture limits. Hence, irrigation starts when soil moisture has dropped to 20% of the soil field capacity and stops at field capacity, during the irrigation period from 15 May to 15 September each year. In addition to the above, 6 command areas (irrigated areas with a common water source and application methods) were set (Figure 4) and given in Table 2.

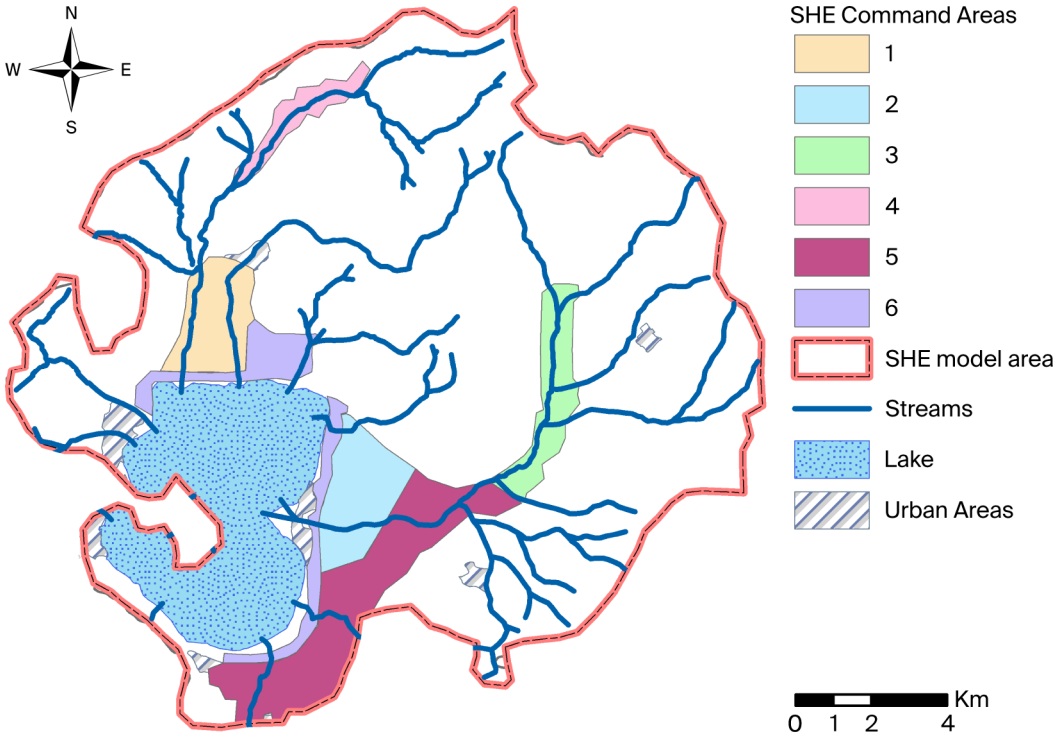


Figure 4. Irrigation command areas in the MIKE SHE hydrological model of the Lake Kastoria catchment.

Table 2. Command areas, their extent (Ha), source of water, and application methods.

Command Area	Extent, Ha	Water Source	Application Method
1	480.0	Vissinia Stream and groundwater	sprinklers
2	1180.0	Groundwater	sprinklers
3	400.0	Xeropotamos Stream and groundwater	sprinklers
4	196.0	Vissinia Stream and groundwater	sprinklers
5	508.0	Groundwater	sprinklers
6	452.0	Lake Kastoria	basin

For the simulation of surface runoff, values for the Manning coefficient (M) were acquired from [67] for each land use category, ranging from 5 to 75. Initial values for the leakage coefficient (L_c) at the areas inundated from the lake, as well as areas occupied by the city of Kastoria (paved areas), were set to 1×10^{-7} s^{-1} and 1×10^{-9} s^{-1}, respectively. Paved areas in the city were considered impermeable to a percentage of 50% to 70%. Surface runoff from these areas is routed to Foudouklis and Aposkepos Streams, which outflow to the lake (Figure 1).

The soil types (Figure 2) were considered uniform in the vertical direction. The full Richard's equation in every single cell was used for the simulation of the water flow in the unsaturated zone. The relationships between soil moisture, pressure head, and hydraulic conductivity (K_s) are described by Van Genuchten formulas [58]. The vertical discretization into nodes for solving the Richards equation was set to 0.25 m, 1.00 m, and 10.00 m for soil depths 0–3 m, 3–40 m, and 40–90 m, respectively.

A phreatic aquifer, which extends over the entire catchment and rests on an impermeable layer, was considered for the simulation of the saturated zone. Its thickness in the mountainous area, where impermeable rocks predominate, was chosen, as an initial approximation, not to exceed 6.0 m, while for the final selection, a sensitivity analysis was carried out. Instead of the above, in the sub-basins of Fotini, Aposkepos, and Fountouklis Streams, as well as in the northern slopes of the Korissos karstic hills, where surface runoff

is rarely observed [68], the thickness of the aquifer was taken from 30 m to 70 m. In the lowland parts where significant aquifers have been developed in the alluvial deposits, the thickness of the aquifer was taken from 40 m to 120 m [52,53].

Hydraulic conductivity (horizontal, K_x, and vertical, K_y) in the saturated zone was subject to sensitivity analysis. In the mountainous part of the basin, initial values as well as their spatial distribution were acquired from the corresponding values of K_s in the unsaturated zone (K_y was equal to K_s). In this case, K_x values were increased by an order of 10 ($K_x = K_y \times 10$). In the lowland part of the basin where the main aquifers are located, initial values were acquired from [51,52].

The initial water table at the lowland was set following [53], while in the mountainous area it was set 2.0 m below the soil surface (almost at the level of the stream's bed).

Subsurface drainage was included in the model and applied to cells adjacent to the streams as well as in agricultural areas where extensive drainage networks are present. The drainage level was set 1.5 m below the soil's surface, while the initial value of the drainage coefficient was set to $C_{dr} = 2.5 \times 10^{-7}$ s^{-1}. This coefficient was subject to sensitivity analysis.

Two types of external groundwater boundary conditions were used: fixed head and zero flux. The fixed head boundary condition was used at (Figure 1): (a) the SE side of the basin, alongside its contact with the Korissos karstic hills, (b) the outlet of the basin, and (c) the west part of the lake where it contacts the limestone of the Peninsula and its extent to the west (west karstic rocks). Throughout the remaining parts of the basin boundary, the zero flux boundary type was adopted.

2.5. MIKE HYDRO River Model Setup

Lake Kastoria and the 9 major streams in the catchment have been included in the MHR model through their 20 branches (Figure 1). Lake Kastoria consists of three branches (Lake, Lake Upper, and Lake Lower), the Visinia Stream has two branches (Visinia and Vitsi), and the Xeropotamos Stream consists of 8 branches, as can be seen in Figure 1. All the above branches were digitized using the MIKE SHE model DTM. This ensures, in terms of shape, position, and slope, compatibility and thus fully hydraulic connectivity between streams, surface waters, and the saturated zone in the MIKE SHE model.

Representative cross-sections were introduced for the branches, the number of which varied according to their length and the topography. In the mountainous as well as in small, shallow streams (e.g., Istakos), their cross-sections were approximated by a simple triangular shape. In contrast, in the lowland sections of the main streams, trapezoidal cross-sections were adopted, since they predominate. The dimensions and shape of the cross-sections were obtained after field visits to the streams (where possible) and through Google Earth images.

The shape and geometry of Lake Kastoria were simulated through 58 cross-sections (Figure 5). The distance between them was taken to be equal to or less than 200 m (the cell size), allowing for the full representation of the lakebed elevation in the MHR environment.

For each cross-section, its Manning's coefficient (n) was set, which is valid downstream up to the next cross-section. This friction was set equal to n = 0.04 [69] for all branches and for the lake.

As the initial condition at the beginning of the simulation (1 November 2012), the LSE, H = 626.82 m a.m.s.l. was set for all lake branches, while a water depth of 0.2 m was set for the streams.

In all upstream open ends of the branches, Q = 0 m^3/s is the boundary condition. Exceptions were the stream of Istakos and the Lake Upper and Lake Lower branches. Istakos receives the discharge of the homonymous karstic spring, which drains a part (515 Ha) of the Korissos limestone rocks. Its mean yearly discharge was estimated to be

Q = 0.066 m^3/s (for a mean yearly rainfall of 736 mm). Lake Upper and Lake Lower upstream ends receive runoff from the part of Kastoria city that has not been included in the model (84 Ha). This runoff outflows directly to the lake and is estimated as 70% of each rainfall event in the catchment.

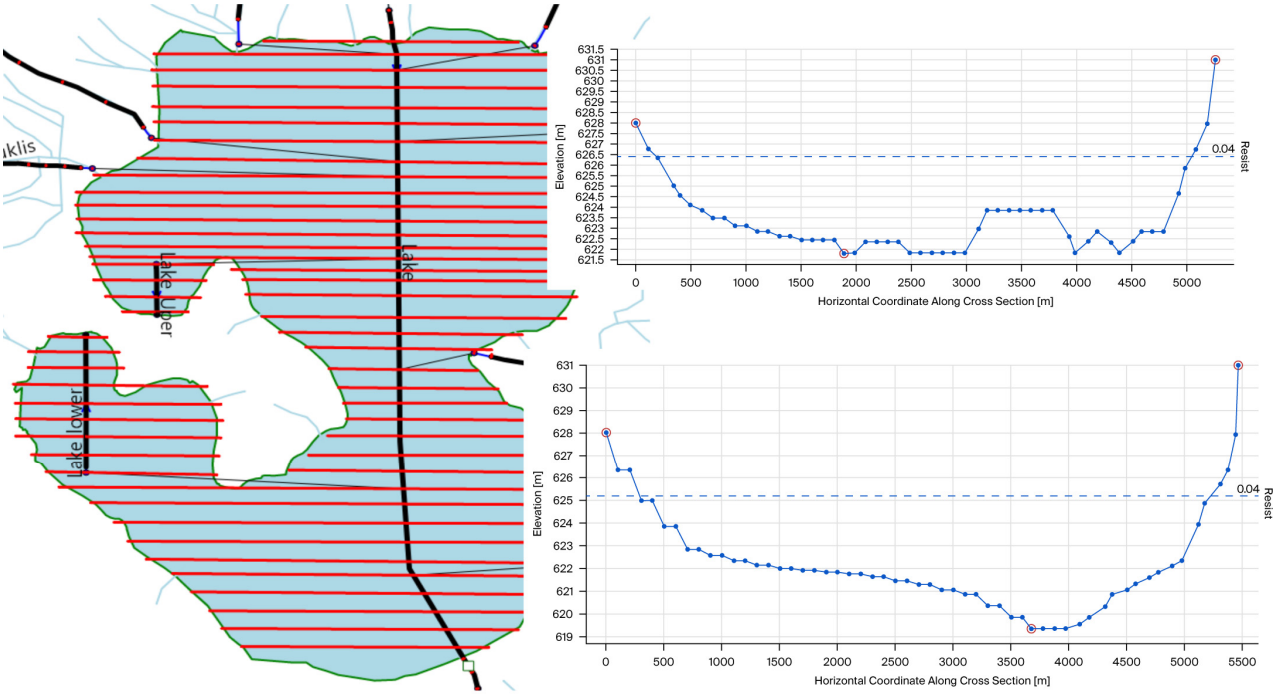


Figure 5. Lake Kastoria cross-sections setup and representative profiles of cross-sections in the hydrological model of its catchment.

At the outlet of the Gioli stream, a constant water level boundary condition was set (H = 615 m a.m.s.l.), which ensures a permanent flow depth at this location of y = 1.0 m. Due to the slope of this branch, this boundary condition does not cause water inflow into the model even if the water level upstream is very low (e.g., during summer).

Furthermore, two additional point-source boundaries were introduced at intermediate locations in the Visinia and Aposkepos Streams (water discharge of 0.032 m^3/s and 0.033 m^3/s, respectively). These conditions relate to the drainage of the Kazani karstic mass (506 Ha), with an average annual discharge of Q = 0.065 m^3/s.

To simulate the operation of the sluice gate, at the outlet of the lake, a "direct discharge" hydraulic structure was used [48]. This virtual hydraulic structure was chosen because it allows: a) to avoid the input of the gate structural elements/dimensions into the model and b) to directly control the outflow discharge through the gate rather than through its operation, e.g., height and duration of its opening through time. Since the operation of the sluice gate is not known (under which conditions it opens and closes), the outflow discharge through the hydraulic structure was chosen to be calculated in such a way that the simulated lake water level (Hsim, m a.m.s.l.) does not exceed the observed level (Hobs, m a.m.s.l.), taking into account that the maximum outflow discharge is 3.3 m^3/s.

2.6. Coupling MIKE SHE and MIKE HYDRO River Models

The lake, together with all streams and their branches, was included in the coupled model of MIKE SHE/MHR (Figure 1). The coupling of the lake was conducted using flood codes in the MIKE SHE environment [58,59]. For all the other branches, whose cross-sections is much smaller than the cell size, the direct overbank spilling was adopted, keeping the default values for the required parameters [58,59].

In the case of the streams, conductance C (m^2/s), for calculating exchange flow between saturated zone grid cells and the river links, was considered to depend on both the leakage coefficient (L_c, s^{-1}) of riverbed material and the hydraulic conductivity (K_x, m/s) of the aquifer material, for all branches. In the case of the lake (branches: Lake, Lake Upper, and Lake Lower), conductance C was considered to depend only on the leakage coefficient of its bed material (initial value $L_c = 1 \times 10^{-7}$ s^{-1}).

For Aposkepos and Foundouklis branches, the initial value for the leakage coefficient was set as $L_c = 1 \times 10^{-5}$ s^{-1}, due to the highly permeable soils in their area. The same value was adopted for the lower part of Xeropotamos from its outlet up to 6.63 km upstream. Along this section, Xeropotamos recharges groundwater in the catchment [52] (personal observation). For all the other branches, the initial value for the leakage coefficient was set as $L_c = 1 \times 10^{-7}$ s^{-1}.

All the above leakage coefficients for both streams and the lake were subject to sensitivity analysis).

2.7. Performance Statistics

A number of statistical criteria were used for the evaluation of the performance of the model (Table 3). They included the correlation coefficient (CC), percent bias (PBias), root mean square error (RMSE), mean error (ME), mean absolute error (MAE), standard deviation of residuals (STD_{res}), and the Nash–Sutcliffe coefficient (NSE − R^2).

Table 3. Statistical criteria for the evaluation of the model's performance and their optimal values.

Formula	Opt. Value
$CC = \frac{\sum_{i=1}^{n}(x_i - \overline{x})(y_i - \overline{y})}{\sqrt{\sum_{i=1}^{n}(x_i - \overline{x})^2 \sum_{i=1}^{n}(y_i - \overline{y})^2}}$	1
$PBias = \frac{\sum_{i=1}^{n}(x_i - y_i)}{\sum_{i=1}^{n} y_i} \times 100$	0
$RMSE = \sqrt{\frac{1}{n}\sum_{i=1}^{n}(x_i - y_i)^2}$	0
$ME = \frac{1}{n}\sum_{i=1}^{n}(x_i - y_i)$	0
$MAE = \lvert ME \rvert$	0
$STD_{res} = \sqrt{\frac{\sum((x_i - y_i) - (\sum(x_i - y_i))/n)^2}{n}}$	0
$NSE - R^2 = 1 - \left[\sum_{i=1}^{n}(y_i - x_i)^2 / \sum_{i=1}^{n}(y_i - \overline{y})^2\right]$	1

Note: n denotes the number of observations; x denotes simulated values; y denotes observed values; and $\overline{x}$ and $\overline{y}$ denote mean values of x and y, respectively.

2.8. Calibration Procedure

The calibration and validation of the model were carried out for the period from 1 November 2012 to 31 December 2022, based mainly on the observed LSE (National Water Monitoring Network of Lakes: "https://wfd.ekby.gr/ (accessed on 14 February 2023)"). Further, but to a lesser degree, they were based on a limited number of observed values of groundwater table (National Water Monitoring Network: "http://nmwn.ypeka.gr/?q=groundwater-stations (accessed on 14 February 2023)" from three boreholes (YKS02, YKS053, and YKS010) around the lake (Figure 1). The observed values of LSE were available, almost on a monthly basis, and covered the whole period of calibration and validation.

In contrast, the observed groundwater table measurements were only available for the months February, July, and October of the years 2013 to 2015 and 2018 to 2020.

The method of split sampling was adopted for the calibration and the validation of the model. The period from 1 November 2012 to 31 December 2019 was used for the calibration, and from 1 January 2020 up to 31 December 2022 for the validation.

The performance of the model was evaluated on the basis of both statistical and qualitative criteria. The statistical criteria are described in Table 3 and were used to calibrate and validate the model against the observed LSE values. The objective in this case was to achieve the optimum values of the above statistical criteria. As qualitative criteria, the range of fluctuation of the modeled groundwater table at the observation wells was used. In this case, the objective was for the fluctuation of the modeled groundwater table to be within the range of fluctuation of its observed values.

Before starting the calibration process, a number of initial simulations were carried out, through which the model was gradually developed, and at the same time, its first parameterization was performed.

The calibration was carried out by the "trial-and-error" method, where the effect of the model parameter values was examined "step by step". This approach enabled an extensive sensitivity analysis of the model, which in turn led to the selection of parameter values under which model performance is better.

No calibration was performed with respect to the models' structural elements (cell size, time step), the effect of which [70–72] has been taken into account for the development of the model. Initial runs of MIKE SHE (for a limited period of one year), with a time step of 30 s (time step at which MIKE HYDRO River is run), did not show significant differences in the results, compared to longer time steps (e.g., up to 1 h). The time step of 1 h was finally adopted for the unsaturated zone (UZ) and overland flow (OL), while for the saturated zone (SZ), the time step of 24 h was used.

2.9. Sensitivity Analysis

The selection of parameters for which sensitivity analysis was performed was based on the specific characteristics of the catchment and previous research work [58,59,71,72], related to the calibration and sensitivity analysis of MIKE SHE models. The selected parameters, the range of their values tested, and the final selected values are given in Tables 4–6. More precisely, the parameters related to real evapotranspiration C_1, C_2, C_3, and AROOT, the depth of SZ lower level in the mountainous area of the catchment, the leakage (L_c) coefficient of Lake Kastoria and river branches, the drainage coefficient (C_{dr}), and the ground water (GW) boundary conditions of the lake are given in Table 4. The values of hydraulic conductivity (ensembles of $K_{x,y}$) of the saturated zone in the mountain part of the catchment are given in Table 5, while in the plain part, in Table 6. The spatial distribution of hydraulic conductivity in the catchment is shown in Figure 6.

Table 4. Calibration parameters, their range of values for which sensitivity analysis was performed, and their final selected values in the hydrological model of the Lake Kastoria catchment.

Parameter	Range of Values Tested	Selected Values
Real Evapotranspiration		
C_1, C_2	0.01, 0.1, 0.3, 0.6, 0.9	0.3, 0.1
C_3 (mm/day)	1, 10, 20, 30	20

Table 4. *Cont.*

Parameter	Range of Values Tested	Selected Values
AROOT	0.1, 0.5, 1.0, 2.0	1.5
Depth of SZ lower level in the m.a *., m	1.5, 2.5, 3.5, 6.0	6.0
Leakage coefficients L_c, s^{-1}		
Vyssinia, Tihio, Metamorphosi	1×10^{-5}, 1×10^{-7}, 1×10^{-9}	1×10^{-7}
Aposkepos, Foudouklis		1×10^{-5}
Fotini, Xeropotamos, Istakos, Gioli		Plain sections: 1×10^{-5} Mountain sections: 1×10^{-9}
Lake Kastoria		1×10^{-7}
Drainage coefficient (C_{dr}, s^{-1})	1×10^{-6}, 1×10^{-7}, 2.5×10^{-7}, 1×10^{-8}, 5×10^{-9}, 1×10^{-9}	1×10^{-7}
GW boundary conditions of the lake, m	+1.00, +1.20	+1.00

* m.a.: mountainous area.

Table 5. Ensembles of $K_{x,y}$ values (m/s) of the saturated zone in the mountainous part of the Lake Kastoria catchment hydrological model, subject to sensitivity analysis, and final selected values.

Ensembles of $K_{x,y}$	**Mountainous Areas Where the Soil Types Are Extended:**		
	Sandy Loam, Loamy Sand, Sandy Clay Loam	**Clay**	**Loam**
1°	$K_x = 0.8 \times 10^{-5}$ $K_y = 0.8 \times 10^{-6}$	$K_x = 4.0 \times 10^{-6}$ $K_y = 4.0 \times 10^{-7}$	$K_x = 2.9 \times 10^{-5}$ $K_y = 2.9 \times 10^{-6}$
2°	$K_x = 1.5 \times 10^{-5}$ $K_y = 1.5 \times 10^{-6}$	$K_x = 4.8 \times 10^{-6}$ $K_y = 4.8 \times 10^{-7}$	$K_x = 2.9 \times 10^{-5}$ $K_y = 2.9 \times 10^{-6}$
3°	$K_x = 1.7 \times 10^{-5}$ $K_y = 1.7 \times 10^{-6}$	$K_x = 5.2 \times 10^{-6}$ $K_y = 5.2 \times 10^{-7}$	$K_x = 2.9 \times 10^{-5}$ $K_y = 2.9 \times 10^{-6}$
4°	$K_x = 5 \times 10^{-5}$ $K_y = 5 \times 10^{-6}$	$K_x = 8.5 \times 10^{-6}$ $K_y = 8.5 \times 10^{-7}$	$K_x = 2.9 \times 10^{-5}$ $K_y = 2.9 \times 10^{-6}$
Finally Selected values	$Kx = 5 \times 10^{-5}$ $Ky = 5 \times 10^{-6}$	$Kx = 8.5 \times 10^{-6}$ $Ky = 8.5 \times 10^{-7}$	$Kx = 2.9 \times 10^{-5}$ $Ky = 2.9 \times 10^{-6}$

Table 6. Ensembles of $K_{x,y}$ values (m/s) of the saturated zone in the plain part of the Lake Kastoria catchment hydrological model, subject to sensitivity analysis, and final selected values.

Ensembles of $K_{x,y}$	Plain Area and Subareas of the Main Aquifer (Figure 6)					
	Lake Bottom	Peninsula Karst	Western Karst	ϒKS020	ϒKS053	ϒKS010
1°	$K_x = 6.9 \times 10^{-6}$, $K_y = 6.9 \times 10^{-6}$	$K_x = 1 \times 10^{-4}$, $K_y = 1 \times 10^{-5}$	$K_x = 5 \times 10^{-5}$, $K_y = 5 \times 10^{-6}$	$K_x = 1 \times 10^{-3}$, $K_y = 1 \times 10^{-4}$		
2°				$K_x = 1 \times 10^{-4}$, $K_y = 1 \times 10^{-5}$		
3°				$K_x = 7.5 \times 10^{-5}$, $K_y = 7.5 \times 10^{-6}$		
4°				$K_x = 5 \times 10^{-5}$, $K_y = 5 \times 10^{-6}$		
5°				$K_x = 2.5 \times 10^{-5}$, $K_y = 2.5 \times 10^{-6}$		
6°				$K_x = 1.0 \times 10^{-6}$, $K_y = 1.0 \times 10^{-7}$		
7°				$K_x = 2.5 \times 10^{-5}$, $K_y = 2.5 \times 10^{-6}$	$K_x = 5 \times 10^{-5}$, $K_y = 5 \times 10^{-6}$	$K_x = 2.5 \times 10^{-5}$, $K_y = 2.5 \times 10^{-6}$
Finally Selected values	$K_x = 6.9 \times 10^{-6}$, $K_y = 6.9 \times 10^{-6}$	$K_x = 1 \times 10^{-3}$, $K_y = 1 \times 10^{-4}$	$K_x = 5 \times 10^{-5}$, $K_y = 5 \times 10^{-6}$	$K_x = 2.5 \times 10^{-5}$, $K_y = 2.5 \times 10^{-6}$	$K_x = 5 \times 10^{-5}$, $K_y = 5 \times 10^{-6}$	$K_x = 2.5 \times 10^{-5}$, $K_y = 2.5 \times 10^{-6}$

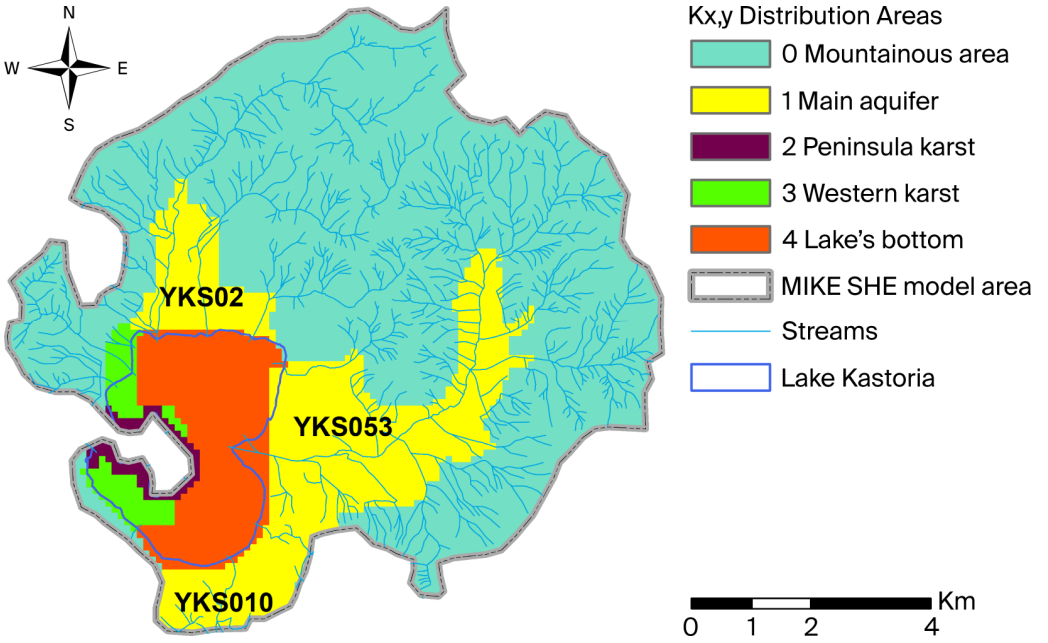


Figure 6. Spatial distribution of hydraulic conductivity in the saturated zone of the Lake Kastoria catchment hydrological model (0: mountainous area; 1: main aquifer in the plain area; 2: Karst of the Peninsula; 3: Western Karst; 4: Lake Bottom; ϒKS020, ϒKS053, and ϒKS010: sub-areas of the main aquifer 1).

3. Results

3.1. Performance and Validation of the Model

The comparison of the observed and simulated LSE of Lake Kastoria using ground weather station data (Base scenario) is shown in Figure 7 for both the calibration and validation period.

During the calibration period, the very good performance of the model is obvious, where the simulated water level very accurately follows both the seasonal changes and the observed values of the LSE. However, in the validation period, although the model follows the seasonal pattern, it underestimates the water level in 2020 and less so in 2021, whereas in 2022, the simulated water level appears to be very satisfactory.

The above picture is also reflected in the quantitative evaluation of the model, which is carried out on the basis of the values of the statistical criteria of Tables 3 and 7.

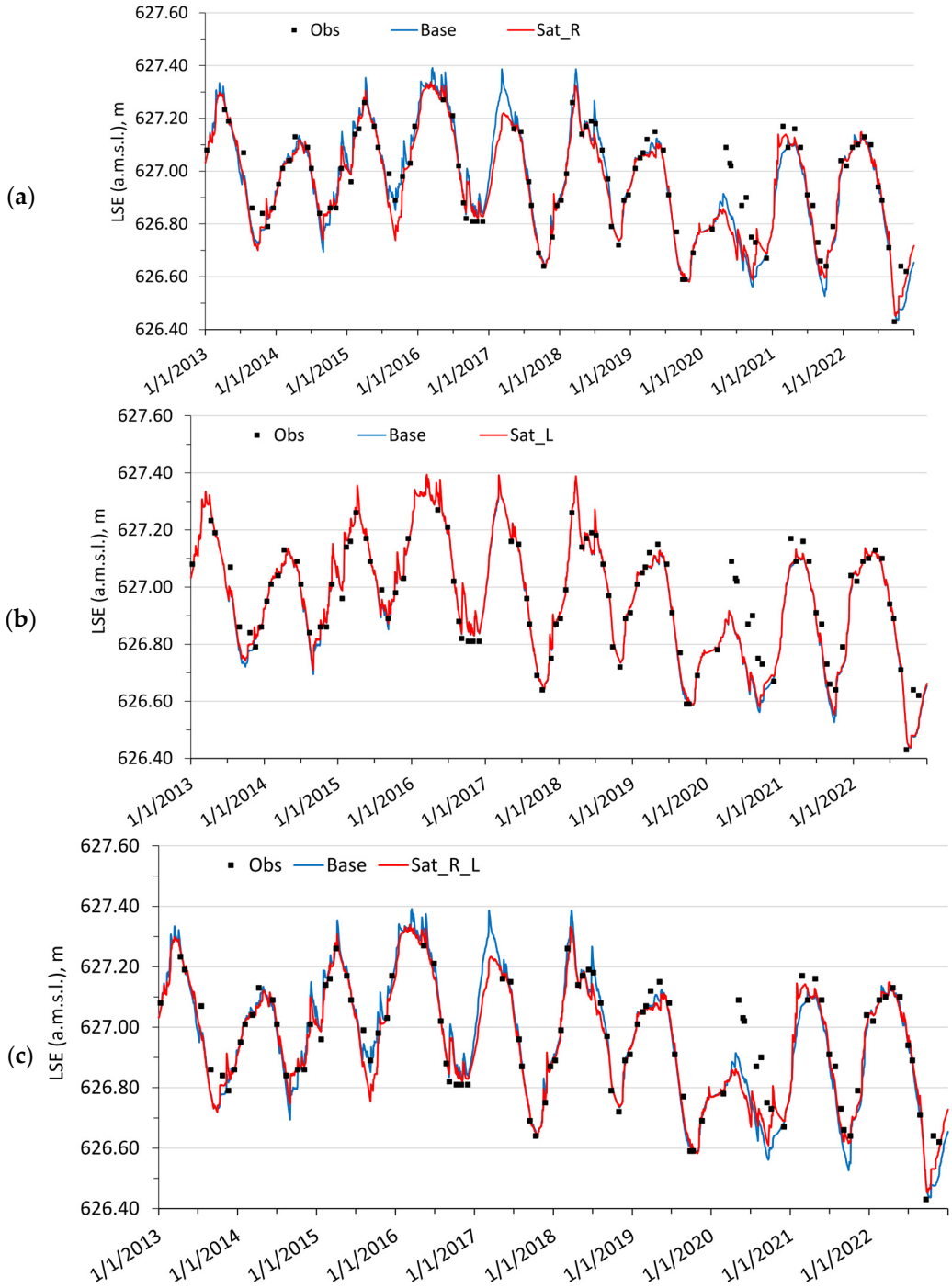


Figure 7. Observed (Obs) and simulated LSE of Lake Kastoria following Base and Sat_R (**a**), Sat_L (**b**), and Sat_R_L (**c**) scenarios of using satellite data of precipitation and LAI in the hydrological model of the Lake Kastoria catchment for the period 2013–2022.

Table 7. Optimum (opt) and estimated values of the statistical evaluation criteria of the Lake Kastoria catchment model (Base scenario) during its calibration (cal) and validation (val) processes.

	ME	MAE	RMSE	STD_{res}	CC	NSE − R^2	R^2	Pbias
opt	0	0	0	0	1	1	1	0
cal	−0.002	0.027	0.035	0.035	0.979	0.958	0.958	0.000
val	0.071	0.080	0.106	0.080	0.926	0.701	0.857	−0.011

With regard to the calibration period, the values of ME and MAE are in the order of 2 mm and 3 cm, while RMSE and STD_{res} do not exceed 3.5 cm. Equally satisfactory (0.979 and 0.958) are the values of CC and R^2, respectively, as well as of the NSE − R^2 coefficient (0.958), which tend towards their optimum values.

In the case of the validation period, the underestimation of the LSE by the model is reflected in the negative value of the Pbias (−0.011). The mean error (ME and MAE) is in the order of 7 cm (12.73%) and 8 cm (14.55%), respectively, when the mean annual variation in the LSE in this period is 55 cm.

The above values are greater and hence worse than the corresponding values in the calibration period. The mean deviation between calculated and observed level values is RMSE = 0.106, and the standard deviation of the error is STD_{res} = 0.08, both quite close to their optimum values of 0. CC, NSE − R^2, and R^2 are quite high and close to their optimum values, although lower than the corresponding values in the calibration period.

The underestimation of the LSE by the model during the validation period can be explained by taking into account the annual rainfall in the catchment (Figure 8).

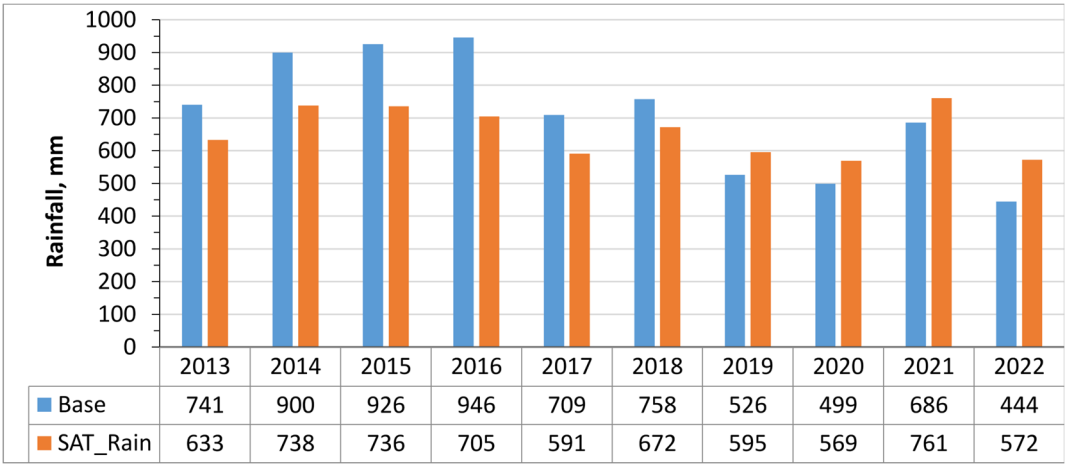


Figure 8. Annual rainfall (mm) at the terrestrial part of the Lake Kastoria catchment, as calculated from the Base and Sat_R models.

The model was calibrated with annual rainfall heights greater than 600 mm. Only in the last year of the calibration period (2019), the rainfall was 526 mm. Observing the simulated LSE in the period 2013–2019 shows that the simulated water level is particularly good (Figure 7). The fact that a relatively rainy year (758 mm) follows a relatively dry year (526 mm) does not seem to affect the model's behavior. However, in the case where the previous year is also relatively rainless (e.g., 2019–2020), it appears that the model underestimates the LSE. This can be attributed to the depletion of the saturated zone in the mountain areas, where its thickness was set to 6 m. Consecutive years of low rainfall led to a progressive depletion of this zone, which minimizes or even eliminates the baseflow to the mountain streams. In turn, this reduces or eliminates the inflow to the main streams that feed the lake, ultimately preventing the lake's water level from recovering.

The comparison of the observed and simulated (Base scenario) water table at the observation sites around the perimeter of the lake is shown in Figure 9 for both calibration and validation periods and seems to be very satisfactory. During calibration, at all three observation sites, the simulated water table is both at the same level as the observed values and within the range of their variation, which was the objective of the model calibration with respect to the groundwater level. In the first two years, the model did not seem to be able to satisfactorily follow the observed values at the observation sites, YKS02 and YKS053. This could be attributed to the initial conditions used, but also to the warming up of the model. On the contrary, the above weakness is not present at location YKS010. At this location, there is a lag in the tracking of the observed level by the model, which could be explained, on the one hand, by the start time of the irrigation (estimated by the model on the basis of the moisture in the soil) and, on the other hand, by the increased quantities of water pumped, which means that the simulated aquifer cannot recover faster than the observed rate.

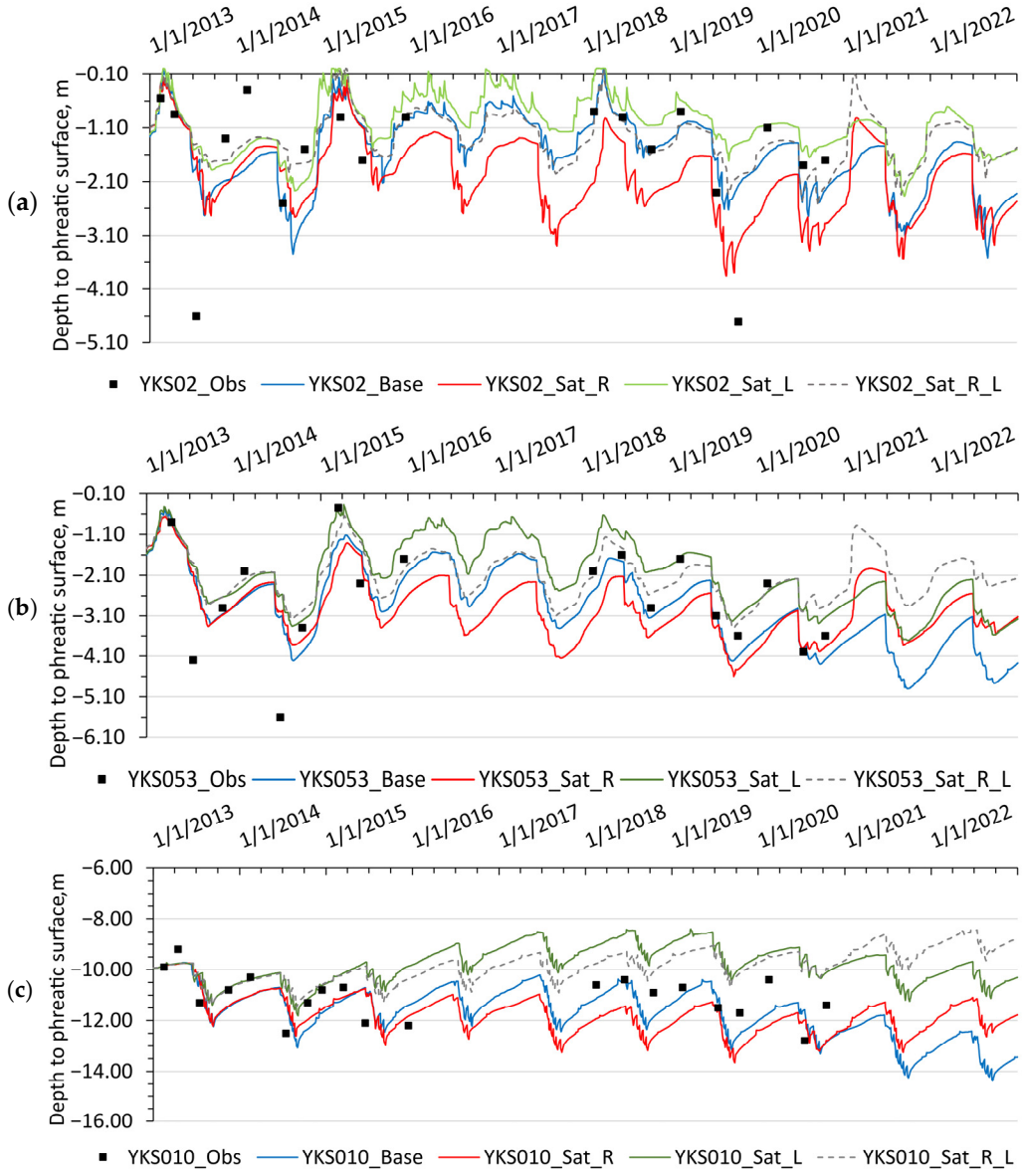


Figure 9. Observed (_Obs) and simulated values of the water table at the observation sites YKS02 (**a**), YKS053 (**b**), and YKS010 (**c**), following Base, Sat_R, Sat_L, and Sat_R_L scenarios, for the period 2013–2022.

In the case of the validation period, the model slightly underestimates the water table by a constant magnitude (depending on the observation location). However, at all three observation sites, the simulated groundwater level is almost at the same level as the observed values, with a very small deviation.

3.2. Prediction of the Lake Kastoria Surface Elevation Using the Calibrated Model, Satellite Precipitation, and LAI Data

The ability of the calibrated model to predict LSE using satellite data instead of ground station precipitation and typical values of LAI for northern Greece (Base scenario) was tested through three additional scenarios. In the first one (Sat_R), satellite precipitation data were used in the calibrated model. In the second one (Sat_L), satellite-derived LAI values, and in the third (Sat_R_L) both satellite precipitation and LAI values were used. All scenarios utilized satellite data corresponding to the period 1 January 2013–31 December 2022.

In the Sat_R scenario, daily precipitation values obtained from the GPM_3IMERGDF were used to replace those from the Kastoria weather station. Additionally, instead of applying hypsometric zoning within the catchment and estimating precipitation using lapse rates, the spatial distribution of the precipitation from the satellite product was employed (Figure 10). In the Sat_L scenario, LAI values for each land-use category were obtained from the GEOV3 dataset. From the above, mean values were extracted for the period 2013–2019 and were used in place of the typical LAI values for the area. The temporal distribution of the above values was defined at ten-day intervals throughout the year and remained constant across all years of the study period. The Sat_R_L scenario combined the modifications introduced in both Sat_R and Sat_L. Specifically, the Base model was driven by both satellite-derived precipitation and LAI data, incorporating their respective spatial and temporal distributions.

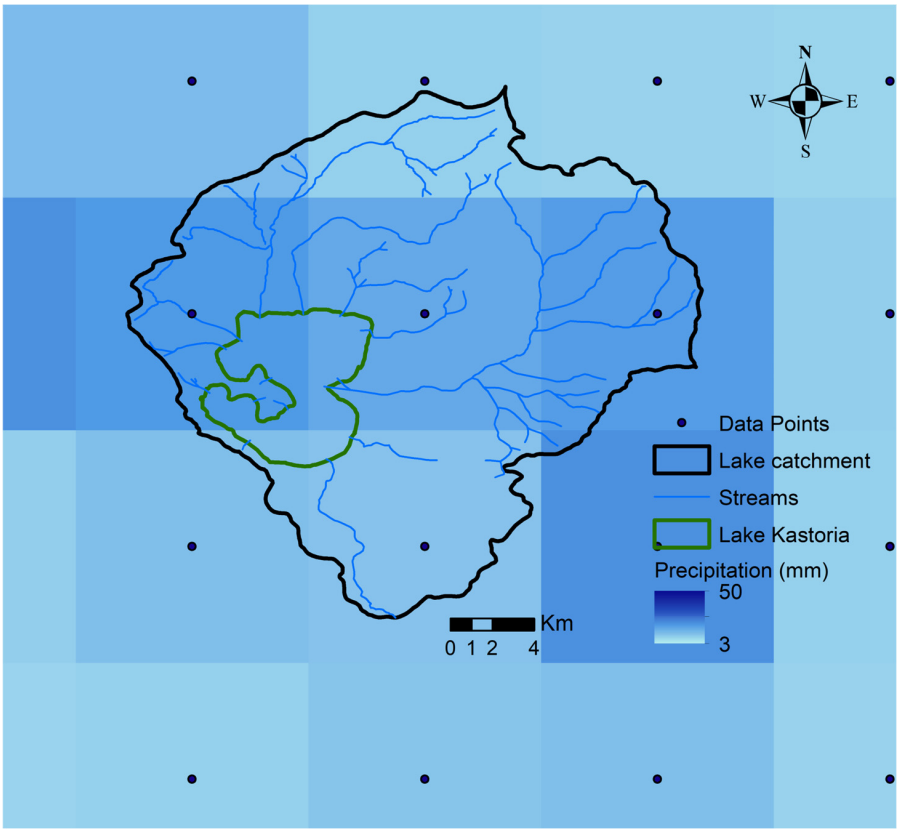


Figure 10. Spatial distribution of the GPM_3IMERGDF product precipitation (6 January 2012) in the Lake Kastoria catchment following Sat_R, and Sat_R_L scenarios.

The effect of the satellite data on the ability of the model to predict the LSE is shown in Figure 7, where the results from each scenario (Sat_R, Sat_L, and Sat_R_L) are compared with the results of the Base and the observed values of Kastoria LSE. As can be seen (Figure 7a), in the Sat_R scenario, the model provides an accurate prediction of the observed LSE, with the exception of the year 2020, as with the Base model. Furthermore, it seems to underestimate the LSE at some peaks and troughs compared to the Base model. In the case of Sat_L (Figure 7b), the LSE is nearly identical to that of the Base model. This indicates that the satellite-derived LAI does not substantially affect the model. Finally, the LSE is predicted very accurately in the Sat_R_L scenario (Figure 7c), where some peaks and troughs have been corrected.

The above comparison between the observed and the predicted in the scenarios LSE is quantified by the values of the corresponding statistical evaluation criteria in Table 8.

Table 8. Statistical evaluation of the performance of Sat_R, Sat_L, and Sat_R_L scenarios, against the hydrological model (Base scenario) of the Lake Kastoria catchment for the period 2013–2022.

Criterion	Optimum Value	Base	Sat_R	Sat_L	Sat_R_L
ME	0	0.021	0.026	0.017	0.021
MAE	0	0.043	0.044	0.041	0.041
RMSE	0	0.066	0.069	0.062	0.065
STD_{res}	0	0.063	0.064	0.060	0.062
CC	1	0.949	0.941	0.951	0.944
NSE − R^2	1	0.870	0.858	0.883	0.873
R^2	1	0.900	0.885	0.904	0.944
PBias	0	−0.003	−0.004	−0.003	−0.003

As can be seen, the differences are very small. The mean absolute error is of the order of 4.4 cm to 4.1 cm (5.2 to 4.9%) for the scenarios and 4.3 cm (5.12%) for the Base model, when the mean annual LSE variation is 84 cm. The dispersion of the error is very low (from 6.9 to 6.2 cm), as shown by the values of the RMSE and STD_{res} criteria. The R^2 and NSE − R^2 criteria of the models are also very good and similar to the best values of Sat_L (R^2 = 0.904 and NSE − R^2 = 0.883). In addition, the models seem to slightly underestimate the LSE following the negative values of PBias.

The effect of using satellite data on the groundwater level in the vicinity of the lake is shown in Figure 9. Regarding Sat_R at all three observation wells, the groundwater level is underestimated—from 0.5 m to 1.0 m—compared to the calculated values from the Base scenario, up to the year 2020. In the following years, there is an almost identical (observation site YKS02) or slightly overestimation (up to 1.00 m), by Sat_R. This behavior can be interpreted from Figure 8, which shows the annual rainfall heights, in the terrestrial part of the catchment (excluding the lake), as calculated in the Base and Sat_R scenarios. From Figure 8, it can be seen that from 2013 to 2018, the rainfall height in the Sat_R scenario is lower than the rainfall in the Base scenario. This pattern begins to change, with a slight difference in 2019, at the expense of the rainfall height of the Base model, to continue until 2022.

In the case of Sat_L, at all three observation sites, there is a slight overestimation of the groundwater level, which increases over time (e.g., at locations YKS02 and YKS010), reaching 0.5 m to 2.0 m, depending on the location. This behavior can be explained by the fact that satellite LAI values are lower than the typically used values, in several land use categories, but mainly in irrigated ones such as orchards and complex cropping systems. This results in lower evapotranspiration in these areas and, consequently, in lower amounts of water pumping for irrigation.

In the case of Sat_R_L, the groundwater table in the area of YKS02 appears to closely follow that of the Base scenario. In contrast, in the other two areas, from 2018 onwards, the

level calculated by Sat_R_L begins to differ from that of the base model, either remaining at the same level (e.g., YKS053) or rising steadily, as in the area of YKS010. The difference between the two levels appears to be small on an annual basis, but nevertheless has an additive effect. An explanation for this differentiation can be found in the pattern of rainfall differences (ground station versus satellite), as shown in Figure 8.

Tables 9 and 10 show the water balance of the lake and the terrestrial part of its catchment, respectively, as calculated from the hydrological models Base, Sat_R, Sat_L, and Sat_R_L.

Table 9. Components of the water balance of the terrestrial part of the Lake Kastoria catchment and their average values for the period 2013–2022, as derived from the Sat_R, Sat_L, and Sat_R_L scenarios and their deviation (Δ = Sat_ − Base, %) from the Base scenario.

		Base	Sat_R	Δ	Sat_L	Δ	Sat_R_L	Δ
	Components	**m^3**	**m^3**					**%**
INFLOWS	Rainfall	165,021,250	152,025,440	−7.88	165,021,259	0.00	*152,025,426*	−7.88
	Snow	204,345	165,957	−18.79	204,336	0.00	165,959	−18.78
	Karstic springs:							
	Kefalari	1,040,688	1,040,688	0.00	1,040,688	0.00	1,040,688	0.00
	Aposkepos	1,009,152	1,009,152	0.00	1,009,152	0.00	1,009,152	0.00
	Istakos	2,081,376	2,081,376	0.00	2,081,376	0.00	2,081,376	0.00
	Groundwater inflows:							
	Korissos hills and Lake	793,914	774,137	−2.49	428,619	−46.01	411,742	−48.14
	Groundwater storage change	2,064,154	3,317,373	60.71	1,885,432	−8.66	3,196,307	54.85
	Total Inflow	**172,214,880**	**160,414,122**	**−6.85**	**171,670,861**	**−0.32**	**159,930,651**	**−7.13**
OUTFLOWS	Evapotranspiration	143,793,876	140,389,056	−2.37	141,859,939	−1.34	138,505,240	−3.68
	Lateral outflow (overland)	2,432,241	2,333,724	−4.05	2,848,552	17.12	2,791,824	14.78
	Outflow from streams	24,910,273	16,492,915	−33.79	25,256,858	1.39	16,811,885	−32.51
	Groundwater discharge:							
	To the lake	2,247,023	2,260,929	0.62	2,482,896	10.50	2,257,124	0.45
	Out from the catchment	231,320	231,320	0.00	231,320	0.00	462,640	100.00
	Groundwater storage change	0	0		0		0	
	Total Outflow	**173,614,733**	**161,707,944**	**−6.86**	**172,679,565**	**−0.54**	**160,828,712**	**−7.36**
	WATER BALANCE	**−1,399,853**	**−1,293,822**	**−7.57**	**−1,008,704**	**−27.94**	**−898,061**	**−35.85**

Table 10. Components of the water balance of Lake Kastoria, their average values for the period 2013–2022, as derived from the Sat_R, Sat_L, and Sat_R_L scenarios and their deviation (Δ = Sat_ − Base, %) from the Base scenario.

		Base	Sat_R	Δ	Sat_L	Δ	Sat_R_L	Δ
	Components	**m^3**	**m^3**	**%**	**m^3**	**%**	**m^3**	**%**
INFLOWS	Rainfall	17,521,227	19,339,777	10.38	17,521,226	0.00	19,339,785	10.38
	Direct runoff from the city	350,730	385,874	10.02	350,730	0.00	385,874	10.02
	Groundwater discharge							
	Lake springs (Karstic)	11,699,321	11,711,112	0.10	11,565,738	−1.14	11,572,159	−1.09
	aquifers	2,247,023	2,260,929	0.62	2,482,896	10.50	2,257,124	0.45
	Lateral inflow (overland)	2,498,995	2,479,424	−0.78	2,922,412	16.94	2,940,840	17.68
	Inflow from streams	24,910,273	16,492,915	−33.79	25,256,858	1.39	16,811,885	−32.51
	Total Inflow	**59,227,569**	**53,957,116**	**−8.90**	**60,099,861**	**1.47**	**53,307,667**	**−10.00**
OUTFLOWS	Evaporation	38,685,921	38,675,116	−0.03	38,687,607	0.00	38,676,562	−0.02
	Infiltration	0	0		0		0	
	Groundwater recharge	464,263	447,329	−3.65	307,907	−33.68	290,967	−37.33
	Lateral outflow (overland)	0	0		0		0	
	Outflow to Gioli	20,355,442	13,701,455	−32.69	21,716,601	6.69	15,060,021	−26.01
	Abstractions—irrigation	1,210,653	1,133,216	−6.40	897,500	−25.87	816,114	−32.59
	Total Outflow	**60,716,278**	**53,957,116**	**−11.13**	**61,609,615**	**1.47**	**54,843,664**	**−9.67**
	WATER BALANCE	**−1,488,709**	**−1,287,086**	**−13.54**	**−1,509,755**	**1.41**	**−1,535,997**	**3.18**

At the catchment level (Table 9), in the case of the Sat_R scenario, rainfall and snowfall are decreased by 7.88% and 18.19%, respectively, which in turn reduces the outflow from the streams to the lake by 33.70%. Snowfall represents a negligible amount (0.11%) of rainfall, as in the case of the Base scenario (0.12%). This great percentage of outflow reduction could be further explained by the significant increase (60.71%) of groundwater storage change in the catchment. The above changes are reflected in the value of the runoff coefficient of the catchment (n_s) as it is described in Equation (1), which was calculated to 0.16 and 0.12 for the Base and Sat_R scenarios, respectively. Minor changes to the rest of the water balance components are observed between the Base and Sat_R scenario.

$$n_s = \frac{(Lateral\ outflow(overland) + Outflow\ from\ streams)}{(Rainfall + Snow + Karstic\ springs)} \quad (1)$$

In the case of the Sat_L scenario, only a minor effect on the water balance of the catchment was observed since the differences in regard to the Base scenario are in the order of −0.32% for the total inflows and −0.54% for the total outflows. A great decrease (−46.01%) is observed regarding the inflows from the Korissos hills and the lake; however, they represent only a minor portion of the total inflow component. Also, increased quantities of lateral outflow (by 17.12%) and groundwater discharge to the lake (by 10.5%) are observed and can be explained by reduced evapotranspiration in the areas close to the lake, which in turn increases available rainfall for surface runoff, groundwater recharge, and outflow to the lake. The runoff coefficient for the catchment was estimated at n_s = 0.17, similar to the expected value for the Base scenario (n_s = 0.16).

In the case of Sat_R_L, a combination of the effects of the two previous scenarios (Sat_R and Sat_L) is observed on the water balance of the catchment, with the Sat_R scenario's effect prevailing by causing a decrease in both total inflows (by −7.13%) and total outflows (by −7.36%). Runoff coefficient was calculated at n_s = 0.13, very close to that of the Sat_R scenario.

In all the above scenarios, the water balance of the catchment is negative (total inflows − total outflows < 0) which implies a depletion of its water resources. This depletion is less in the case of Sat_R by −7.57%, in the case of Sat_L by −27.94%, and in the case of Sat_R_L by −35%. The large shift in the case of the scenarios where satellite LAI values are used can only be explained by smaller amounts of evapotranspiration and its distribution during the year.

The differences in the water balance of the lake's catchment area that come from the above scenarios affect and explain the components of the lake's water balance (Table 10) and the total runoff coefficient of the lake's catchment n_t as given by Equation (2).

$$n_t = \frac{(Outflow\ to\ Gioli)}{(Rainfall + Snow + Karstic\ springs + Lake\ springs)} \quad (2)$$

In the case of scenarios Sat_R and Sat_R_L, there is a decrease in both inflows (−8.90% and −10.00%) and outflows (−11.13% and −9.67%), with the total runoff coefficient becoming n_t = 0.07 and n_t = 0.08, respectively, compared to the Base coefficient, which is n_t = 0.1. These conditions, as mentioned above, are justified by the reduced amount of rain and snow in the basin and, consequently, the reduced inflows into the lake (Table 10).

In contrast, in the Sat_L scenario, both total inflows and outflows are marginally increased by +1.47% (in both cases) compared to the corresponding quantities in the Base, while the total runoff coefficient was found to be n_t = 0.11, very close to that of the Base (n_t = 0.1).

In the case of the lake, as in that of its catchment, the balance is negative (Total Inflow − Total Outflow < 0), which indicates a drop in its level at the end of the year. Taking into account a mean surface area of the lake (2944.0 ha), the average annual drop in its water level is estimated at 0.05, 0.04, 0.05, and 0.05 m for the Base, Sat_R, Sat_L, and Sat_R_L scenarios, respectively.

4. Conclusions

The aim of the present study was to demonstrate the effectiveness of the fully distributed hydrological models in combination with the use of satellite data for estimating the long-term water level fluctuation of natural lakes under the specific conditions prevailing in Greece. For this purpose, we used the coupled MIKE SHE/MHR hydrological modeling system in combination with satellite precipitation and LAI data from the products GPM_3IMERGDF and GEOV3, respectively.

The study showed that the above system provided the potential to embed in the hydrological model of Kastoria Lake catchment with high spatial resolution: (a) the physiographic characteristics of the catchment and the geometry of its lake and streams, (b) the management of water resources in the catchment, e.g., extent and location of irrigated areas, irrigation methods and water sources spatially distributed, (c) Lake Kastoria, as a structural element of its catchment, but also of its dynamic interaction with the neighboring surface and groundwater, and (d) hydraulic structures, like the sluice gate at the outlet of the lake and its operation.

The simulation of the long-term LSE from the model using precipitation data from the ground station and typical for northern Greece values of LAI (Base model) was evaluated as very satisfactory. The reliability of the model performance was substantially enhanced from

the parallel use of observed water table data in the perimeter of the lake as a dual calibration objective. The model seems to underestimate the LSE during periods of consecutive years with low rainfall, which is attributed to the relatively high annual rainfall during its calibration period.

In all cases where satellite data were used (Sat_R, Sat_L, and Sat_R_L scenarios), the simulation of the long-term LSE was very satisfactory, with minor to medium changes to the inflow and outflow components of the water balance in the catchment and the lake. Changes to inflows and outflows in the catchment varied from 0.32 to 7.36%, whereas in the lake, from 1.47 to 11.13%. The above changes were also reflected in the runoff coefficient of both the terrestrial part of the catchment (n_s) and the outlet of the lake (n_t). In particular, their values varied from $n_s = 0.12$ to $n_s = 0.17$ for the first case and from $n_t = 0.07$ to $n_t = 0.11$ for the second one.

In conclusion, the satellite products GPM_3IMERGDF for precipitation and GEOV3 for LAI can adequately be used, instead of ground station precipitation data and the typical values of LAI, in the calibrated hydrological model of the Lake Kastoria catchment for the prediction of the LSE. Furthermore, a plethora of quantified information in relation to the catchment's water balance can be extracted from any of the above scenarios and used in decision-making processes. This positive result makes it tempting the expand this research in other lake catchments for further evaluation of the above products in Greece, given the lack of relevant spatiotemporal data in the country and their importance.

The model's high performance could make it a suitable platform for evaluating the impact of climate change scenarios on lake surface elevation (LSE) or for comparing the effectiveness of precipitation and leaf area index (LAI) of different satellite products, as well as the suitability of satellite products for other parameters, such as soil moisture, actual evapotranspiration, etc.

Author Contributions: Conceptualization, D.P. (Dimitris Papadimos) and D.P. (Dimitris Papamichail); methodology, D.P. (Dimitris Papadimos); software, D.P. (Dimitris Papadimos), D.P. (Dimitris Papamichail); validation, D.P. (Dimitris Papadimos), D.P. (Dimitris Papamichail); formal analysis, D.P. (Dimitris Papadimos); investigation, D.P. (Dimitris Papadimos); resources, D.P. (Dimitris Papadimos); data curation, D.P. (Dimitris Papadimos); writing—original draft preparation, D.P. (Dimitris Papadimos) and D.P. (Dimitris Papamichail); writing—review and editing, D.P. (Dimitris Papamichail); visualization, D.P. (Dimitris Papamichail); supervision. All authors have read and agreed to the published version of the manuscript.

Funding: This research was funded from Act MIS 5001204, financed by the European Union Cohesion Fund (National Strategic Reference Framework 2014–2020), and Acts MIS 371010, 371138, 371140, 371144, 371145, financed by the European Regional Development Fund (National Strategic Reference Framework 2007–2013).

Data Availability Statement: The data are freely available upon request from the corresponding author.

Acknowledgments: This research formed part of the Greek National Water Monitoring Network, according to JMD 107168/1444/2021, implemented by The Goulandris Natural History Museum, Greek Biotope/Wetland Center (EKBY). The network is supervised by the General Directorate for Waters of the Ministry of Environment and Energy. We thank the reviewers and the editor for their comments and recommendations that improved our article.

Conflicts of Interest: The authors declare no conflicts of interest. The funders had no role in the design of the study; in the collection, analyses, or interpretation of data; in the writing of the manuscript; or in the decision to publish the results.

Abbreviations

The following abbreviations are used in this manuscript:

GPM_3IMERGDF	GPM Level 3 IMERG Final Daily 10 × 10 km, V06
GEOV3	VPROVA-V LAI, 300m Version 1.0
HNMS	Hellenic National Meteorological Service
CGLS	Copernicus Global Land Service
LAI	Leaf Area Index
LSE	Lake Surface Elevation
MHR	MIKE HYDRO River
DTM	Digital Terrain Model
WFD	Water Framework Directive
CLC	Corine Land Cover
WL	Water level

References

1. Abbott, M.B.; Bathurst, J.C.; Cunge, J.A.; O'Connell, P.E.; Rasmussen, J. An introduction to the European Hydrological System—Système Hydrologique Européen, "SHE": 1. History and philosophy of a physically-based, distributed modeling system. *J. Hydrol.* **1986**, *87*, 45–59. [CrossRef]
2. Abbott, M.B.; Bathurst, J.C.; Cunge, J.A.; O'Connell, P.E.; Rasmussen, J. An introduction to the European Hydrological System—Système Hydrologique Européen, "SHE": 2. Structure of a physically-based, distributed modeling system. *J. Hydrol.* **1986**, *87*, 61–77. [CrossRef]
3. Refsgaard, J.C.; Storm, B. MIKE SHE. In *Computer Models of Watershed Hydrology*; Singh, V.P., Ed.; Water Resources Publications: Highlands Ranch, CO, USA, 1995; pp. 806–846.
4. Bicknell, B.R.; Imhoff, J.C.; Kittle, J.L., Jr.; Donigian, A.S., Jr.; Johanson, R.C. *Hydrologic Simulation Program—FORTRAN (HSPF): User's Manual for Release 10*; Report No. EPA/600/R-93/174; U.S. EPA Environmental Research Laboratory: Athens, GA, USA, 1993.
5. Arnold, J.G.; Srinivasan, R.; Muttiah, R.S.; Williams, J.R. Large area hydrologic modeling and assessment. Part I: Model development. *J. Am. Water Resour. Assoc.* **1998**, *34*, 73–89. [CrossRef]
6. Feldman, A. *Hydrologic Modeling System HEC-HMS Technical Reference Manual*; U.S. Army Corps of Engineers, Hydrologic Engineering Center: Davis, CA, USA, 2000.
7. Bingner, R.L.; Theurer, F.D.; Yuan, Y. *AnnAGNPS Technical Processes: Documentation Version 2*; Unpublished Report; USDA-ARS National Sedimentation Laboratory: Oxford, MS, USA, 2001.
8. Bouraoui, F.; Braud, I.; Dillaha, T.A. ANSWERS: A nonpoint-source pollution model for water, sediment, and nutrient losses. In *Mathematical Models of Small Watershed Hydrology and Applications*; Singh, V.P., Frevert, D.K., Eds.; Water Resources Publications: Highlands Ranch, CO, USA, 2002; pp. 833–882.
9. Gao, H.; Tang, Q.; Shi, X.; Zhu, C.; Bohn, T.J.; Su, F.; Sheffield, J.; Pan, M.; Lettenmaier, D.P.; Wood, E.F. Water budget record from Variable Infiltration Capacity (VIC) model. In *Algorithm Theoretical Basis Document for Terrestrial Water Cycle Data Records*; University of Washington, Department of Civil and Environmental Engineering: Seattle, WA, USA, 2009; pp. 120–173. Available online: https://eprints.lancs.ac.uk/id/eprint/89407/ (accessed on 17 October 2022).
10. Singh, R.; Subramanian, K.; Refsgaard, C.J. Hydrological modeling of a small watershed using MIKE SHE for irrigation planning. *Agric. Water Manag.* **1999**, *41*, 149–166. [CrossRef]
11. Thompson, J.R.; Iravani, H.; Clilverd, H.M.; Sayer, C.D.; Heppell, C.M.; Axmacher, J.C. Simulation of the hydrological impacts of climate change on a restored floodplain. *Hydrol. Sci. J.* **2017**, *62*, 2482–2510. [CrossRef]
12. Saha, G.C.; Quinn, M. Integrated surface water and groundwater analysis under the effects of climate change, hydraulic fracturing and its associated activities: A case study from northwestern Alberta, Canada. *Hydrology* **2020**, *7*, 70. [CrossRef]
13. Zhang, J.; Zhang, M.; Song, Y.; Lai, Y. Hydrological simulation of the Jialing River Basin using the MIKE SHE model in changing climate. *J. Water Clim. Change* **2021**, *12*, 2495–2514. [CrossRef]
14. Dimitriou, E.; Moussoulis, E. Hydrological and nitrogen distributed catchment modeling to assess the impact of future climate change at Trichonis Lake, western Greece. *Hydrogeol. J.* **2010**, *18*, 441–454. [CrossRef]
15. Papagera, A.; Ioannou, K.; Zaimes, G.; Iakovoglou, V.; Simeonidou, M. Simulation and prediction of water allocation using artificial neural networks and a spatially distributed hydrological model. *AGRIS Line Pap. Econ. Inform.* **2014**, *6*, 101–111.
16. Kourgialas, N.N.; Karatzas, G.P.; Morianou, G. Water management plan for olive orchards in a semi-mountainous area of Crete, Greece. *Glob. Nest J.* **2015**, *17*, 72–81.
17. Papadimos, D.; Demertzi, K.; Papamichail, D. Assessing lake response to extreme climate change using the coupled MIKE SHE/MIKE 11 model: Case study of Lake Zazari in Greece. *Water* **2022**, *14*, 921. [CrossRef]

18. Kourgialas, N.; Morianou, G.; Tzerakis, K.; Malandraki, A.; Psarras, G. Decision-making irrigation system based on MIKE SHE model for addressing water scarcity in Mediterranean olive orchards. In Proceedings of the EGU General Assembly 2023, Vienna, Austria, 24–28 April 2023. [CrossRef]
19. Jarvis, A.; Reuter, I.H.; Nelson, A.; Guevara, E. *Hole-Filled Seamless SRTM Data V4*; International Centre for Tropical Agriculture (CIAT): Cali, Colombia, 2008. Available online: https://srtm.csi.cgiar.org (accessed on 2 November 2020).
20. CLC2012 (Corine Land Cover). European Union's Copernicus Land Monitoring Service Information. 2012. Available online: https://sdi.eea.europa.eu/catalogue/copernicus/api/records/916c0ee7-9711-4996-9876-95ea45ce1d27?language=all (accessed on 14 February 2023).
21. CLC2018 (Corine Land Cover). European Union's Copernicus Land Monitoring Service Information. 2018. Available online: https://sdi.eea.europa.eu/catalogue/copernicus/api/records/71c95a07-e296-44fc-b22b-415f42acfdf0?language=all (accessed on 14 February 2023).
22. Hiederer, R. Mapping Soil Properties for Europe—Spatial Representation of Soil Database Attributes. In *EUR26082EN Scientific and Technical Research Series*; Publications Office of the European Union: Luxembourg, 2013; pp. 2013–2047.
23. Hiederer, R. Mapping Soil Typologies—Spatial Decision Support Applied to European Soil Database. In *EUR25932EN Scientific and Technical Research Series*; Publications Office of the European Union: Luxembourg, 2013; pp. 2013–2147, ISSN 1831-9424.
24. Karatassiou, M.; Ragkos, A.; Markidis, P.; Stavrou, T. A comparative Study of Methods for the Estimation of the Leaf Area in Forage Species. In Proceedings of the 7th International Conference on Information and Communication Technologies in Agriculture, Food and Environment (HAICTA 2015), Kavala, Greece, 17–20 September 2015; pp. 326–332. Available online: http://ceur-ws.org/Vol-1498/HAICTA_2015_paper38.pdf (accessed on 10 November 2020).
25. Aschonitis, V.G.; Papamichail, D.M.; Lithourgidis, A.; Fano, E.A. Estimation of Leaf Area Index and Foliage Area Index of Rice using an Indirect Gravimetric Method. *Commun. Soil Sci. Plant Anal.* **2014**, *45*, 1726–1740. [CrossRef]
26. Kalisperakis, I.; Stentoumis Ch Grammatikopoulos, L.; Karantzalos, K. Leaf Area Index Estimation in Vineyards from UAV Hyperspectral Data, 2D Image Mosaics and 3D Canopy Surface Models. *Int. Arch. Photogramm. Remote Sens. Spat. Inf. Sci.* **2015**, *XL-1/W4*, 299–303. [CrossRef]
27. Campos-Taberner, M.; Garcia-Haro, F.; Camps-Valls, G.; Grau-Muedra, G.; Nutini, F.; Busetto, L.; Katsantonis, D.; Stavrakoudis, D.; Minakou, C.; Gatti, L.; et al. Exploitation of SAR and Optical Sentinel Data to Detect Rice Crop and Estimate Seasonal Dynamics of Leaf Area Index. *Remote Sens.* **2017**, *9*, 248. [CrossRef]
28. Alexandridis, T.K.; Stavridou, D.; Strati, S.; Monachou, S.; Silleos, N. LAI measurement with hemispherical photographs at variable conditions for assessment of remotely sensed estimations. In Proceedings of the ESA Living Planet Symposium, Edinburgh, UK, 9–13 September 2013; Volume 252, p. 722.
29. Chrysafis, I.; Korakis, G.; Kyriazopoulos, A.P.; Mallinis, G. Retrieval of Leaf Area Index Using Sentinel-2 Imagery in a Mixed Mediterranean Forest Area. *ISPRS Int. J. Geo-Inf.* **2020**, *9*, 622. [CrossRef]
30. Ovakoglou, G.; Alexandridis, T. Estimation of the relation between leaf area index and vegetation index from MODIS satellite images across seasons and study areas. In Proceedings of the 9th Panhellenic Congress of the Society of Agricultural Engineers of Greece "Innovation and New Technologies in Agricultural Engineering and Natural Resource Management", Thessaloniki, Greece, 8–9 October 2015; p. 825.
31. Khairul, I.M.; Mastrantonas, N.; Rasmy, M.; Koike, T.; Takeuchi, K. Inter-comparison of gauge-corrected global satellite rainfall estimates and their applicability for effective water resource management in a transboundary river basin: The case of the Meghna River Basin. *Remote Sens.* **2018**, *10*, 828. [CrossRef]
32. Ali, M.H.; Popescu, I.; Jonoski, A.; Solomatine, D.P. Remote sensed and/or global datasets for distributed hydrological modeling: A review. *Remote Sens.* **2023**, *15*, 1642. [CrossRef]
33. Beck, H.E.; Pan, M.; Roy, T.; Weedon, G.P.; Pappenberger, F.; Van Dijk, A.I.; Huffman, G.J.; Adler, R.F.; Wood, E.F. Daily evaluation of 26 precipitation datasets using Stage-IV gauge–radar data for the CONUS. *Hydrol. Earth Syst. Sci.* **2019**, *23*, 207–224. [CrossRef]
34. Andersen, J.; Dybkjaer, G.; Jensen, H.K.; Refsgaard, C.J.; Rasmussen, K. Use of remotely sensed precipitation and leaf area index in a distributed hydrological model. *J. Hydrol.* **2002**, *264*, 34–50. [CrossRef]
35. Fang, H.; Baret, F.; Plummer, S.; Schaepman-Strub, G. An overview of global leaf area index (LAI): Methods, products, validation, and applications. *Rev. Geophys.* **2019**, *57*, 739–799. [CrossRef]
36. Kganyago, M.; Mhangara, P.; Alexandridis, T.; Laneve, G.; Ovakoglou, G.; Mashiyi, N. Validation of sentinel-2 leaf area index (LAI) product derived from SNAP toolbox and its comparison with global LAI products in an African semi-arid agricultural landscape. *Remote Sens. Lett.* **2020**, *11*, 883–892. [CrossRef]
37. Wanders, N.; Bierkens, M.F.; de Jong, S.M.; de Roo, A.; Karssenberg, D. The benefits of using remotely sensed soil moisture in parameter identification of large-scale hydrological models. *Water Resour. Res.* **2014**, *50*, 6874–6891. [CrossRef]
38. Beck, H.E.; van Dijk, A.I.J.M.; Levizzani, V.; Schellekens, J.; Miralles, D.G.; Martens, B.; de Roo, A. MSWEP: 3-hourly 0.25° global gridded precipitation (1979–2015) by merging gauge, satellite, and reanalysis data. *Hydrol. Earth Syst. Sci.* **2017**, *21*, 589–615. [CrossRef]

39. Kittel, C.M.M.; Nielsen, K.; Tøttrup, C.; Bauer-Gottwein, P. Informing a hydrological model of the Ogooué with multi-mission remote sensing data. *Hydrol. Earth Syst. Sci.* **2018**, *22*, 1453–1472. [CrossRef]
40. Jiang, D.; Wang, K. The role of satellite-based remote sensing in improving simulated streamflow: A review. *Water* **2019**, *11*, 1615. [CrossRef]
41. Alfieri, L.; Avantzi, F.; Delogu, F.; Gabellani, S.; Bruno, G.; Campo, L.; Libertino, A.; Massari, C.; Tarpanelli, A.; Rains, D.; et al. High-resolution satellite products improve hydrological modeling in northern Italy. *Hydrol. Earth Syst. Sci.* **2022**, *26*, 3921–3939. [CrossRef]
42. Choi, J.; Kim, U.; Kim, S. Ecohydrologic model with satellite-based data for predicting streamflow in ungauged basins. *Sci. Total Environ.* **2023**, *903*, 166617. [CrossRef]
43. Elhag, M.; Yilmaz, N. Insights of remote sensing data to surmount rainfall/runoff data limitations of the downstream catchment of Pineios River, Greece. *Environ. Earth Sci.* **2021**, *80*, 35. [CrossRef]
44. Sapountzis, M.; Kastridis, A.; Kazamias, A.P.; Karagiannidis, A.; Nikolopoulos, P.; Lagouvardos, K. Utilization and uncertainties of satellite precipitation data in flash flood hydrological analysis in ungauged watersheds. *Glob. Nest J.* **2021**, *23*, 388–399. [CrossRef]
45. Voulanas, D.; Theodossiou, N.; Hatzigiannakis, E. Assessment of potential hydrological climate change impacts in the Kastoria basin (Western Macedonia, Greece) using EURO-CORDEX regional climate models. *Glob. Nest J.* **2021**, *23*, 43–54. [CrossRef]
46. Hrissanthou, V.; Mylopoulos, N.; Tolikas, D.; Mylopoulos, Y. Simulation modeling of runoff, groundwater flow and sediment transport into Lake Kastoria, Greece. *Water Resour. Manag.* **2003**, *17*, 223–242. [CrossRef]
47. Wassem, M.; Schilling, J.; Kachholz, F.; Tranckner, J. Improved representation of flow and water quality in a north-eastern German lowland catchment by combining low-frequency monitored data with hydrological modeling. *Sustainability* **2020**, *12*, 4812. [CrossRef]
48. DHI. *MIKE HYDRO River User Guide*; MIKE Powered by Danish Hydraulic Institute: Hørsholm, Denmark, 2023; p. 362.
49. DHI. *MIKE HYDRO Note to Existing MIKE 11 Users*; MIKE Powered by Danish Hydraulic Institute: Hørsholm, Denmark, 2023; p. 8.
50. Thompson, J.R.; Sørensen, H.R.; Gavin, H.; Refsgaard, A. Application of the coupled MIKE SHE/MIKE 11 modeling system to a lowland wet grassland in southeast England. *J. Hydrol.* **2004**, *293*, 151–179. [CrossRef]
51. Vafiadis, P.P. Hydrogeological Study of the Lake Kastoria Catchment. Ph.D. Thesis, Aristotle University of Thessaloniki, Thessaloniki, Greece, 1983. (In Greek)
52. Yianneli, C.H. Hydrogeological Research in Catchments of Greek Territory. The Example of Agii Anargiri (Kastoria) Catchment. Ph.D. Thesis, Aristotle University of Thessaloniki, Thessaloniki, Greece, 2009. (In Greek)
53. YPAAT. *Monitoring the Chemical Quality of Irrigation Water (Surface and Groundwater) on a River Basin Scale in Macedonia, Thrace and Thessaly. Results of the Kastoria Basin—Hydrogeological Data*; YPAAT: Athens, Greece, 2012; p. 19. (In Greek)
54. Carsel, R.F.; Parrish, R.S. Developing joint probability distributions of soil water retention characteristics. *Water Resour. Manag.* **1988**, *24*, 755–769. [CrossRef]
55. Hou, A.Y.; Kakar, R.K.; Neeck, S.; Azarbarzin, A.A.; Kummerow, C.D.; Kojima, M.; Oki, R.; Nakamura, K.; Iguchi, T. The Global Precipitation Measurement mission. *Bull. Am. Meteorol. Soc.* **2014**, *95*, 701–722. [CrossRef]
56. Huffman, G.J.; Stocker, E.F.; Bolvin, D.T.; Nelkin, E.J.; Tan, J. *GPM IMERG Final Precipitation L3 Half Hourly 0.1 Degree × 0.1 Degree V06*; Goddard Earth Sciences Data and Information Services Center (GES DISC): Greenbelt, MD, USA, 2019. [CrossRef]
57. Smets, B.; Jacobs, T.; Verger, A. *Product User Manual, Leaf Area Index (LAI)—Fraction of Photosynthetically Active Radiation (FAPAR)—Fraction of Vegetation Cover (FCOVER), Collection 300m. GIO-GL LOT 1*; GMES Initial Operations; Copernicus: Göttingen, Germany, 2018.
58. DHI. *MIKE SHE Reference Guide—Volume 2*; MIKE Powered by Danish Hydraulic Institute: Hørsholm, Denmark, 2017; p. 372.
59. Tsombos, P.; Mitropoulos, D.; Ioakeim, C.H.; Zananiri, E.; Zervakou, A.; Nikolakopoulos, K.; Zimianitis, E.; Efthymiou, G.; Dimitriadis, A.L.; Kaminari, M. *Execution of Bathymetric and Sedimentological Surveys on the Bottom of Lake Kastoria*; Report E10963; Institute of Geological and Mineral Research (IGME): Athens, Greece, 2011; Volume A, 409p. (In Greek)
60. Hargreaves, G.H.; Samani, Z.A. Estimating potential evapotranspiration. *J. Irrig. Drain. Eng.* **1982**, *108*, 225–230. [CrossRef]
61. Hargreaves, G.H.; Samani, Z.A. Reference crop evapotranspiration from temperature. *Appl. Eng. Agric.* **1985**, *1*, 96–99. [CrossRef]
62. Papamichail, M.D.; Babatzimopoulos, S.C. *Applied Agricultural Hydraulics*; Ziti Publications: Thessaloniki, Greece, 2014; 568p, ISBN 9789604564156. (In Greek)
63. Aschonitis, V.G.; Papamichail, D.; Demertzi, K.; Colombani, N.; Mastrocicco, M.; Ghirardini, A.; Castaldelli, G.; Fano, E. Highresolution global grids of revised Priestley-Taylor and Hargreaves-Samani coefficients for assessing ASCE-standardized reference crop evapotranspiration and solar radiation. *Earth Syst. Sci. Data* **2017**, *9*, 615–638. [CrossRef]
64. Ministry of Development. *Development of Water Resources Management Systems and Tools for the Water Districts of Macedonia and Thrace*; Special Issue I; ENM Consulting Engineers: Athens, Greece, 2006; p. 55. (In Greek)
65. Kristensen, K.J.; Jensen, S.E. A model for estimating actual evapotranspiration from potential evapotranspiration. *Nord. Hydrol.* **1975**, *6*, 170–188. [CrossRef]

66. Papaioannou, G.; Efstratiadis, A.; Vasiliades, L.; Loukas, A.; Papalexiou, S.M.; Koukouvinos, A.; Tsoukalas, I.; Kossieris, P. An operational method for Flood Directive implementation in ungauged urban areas. *Hydrology* **2018**, *5*, 24. [CrossRef]
67. Hadjimichael, P. *The Catchment Area of Lake Kastoria—Investigation of Flooding Phenomena and Risks Using GIS*; Inter-Institutional Master's Programme "Prevention and Management of Natural Disasters", National and Kapodistrian University of Athens, School of Sciences—Department of Geology and Geoenvironment; Technological Educational Institute of Serres—Department of Geoinformatics & Topography: Athens, Greece, 2011; 204p. (In Greek)
68. Chow, V.T. *Open-Channel Hydraulics; International Student Edition*; McGraw-Hill: New York, NY, USA, 1959; p. 680.
69. Feyen, L.; Vazquez, R.; Christiaens, K.; Sels, O.; Feyen, J. Application of a distributed physically-based hydrological model to a medium size catchment. *Hydrol. Earth Syst. Sci.* **2000**, *4*, 47–63. [CrossRef]
70. Vazquez, R.F.; Feyen, L.; Feyen, J.; Refsgaard, J.C. Effect of grid size on effective parameters and model performance of the MIKE-SHE code. *Hydrol. Process.* **2002**, *16*, 355–372. [CrossRef]
71. Guinot, V.; Gourbesville, P. Calibration of physically based models: Back to basics? *J. Hydroinform.* **2003**, *5*, 233–244. [CrossRef]
72. Vázquez, R.F.; Feyen, J. Effect of potential evapotranspiration estimates on effective parameters and performance of the MIKE SHE code applied to a medium-size catchment. *J. Hydrol.* **2003**, *270*, 309–327. [CrossRef]

Disclaimer/Publisher's Note: The statements, opinions and data contained in all publications are solely those of the individual author(s) and contributor(s) and not of MDPI and/or the editor(s). MDPI and/or the editor(s) disclaim responsibility for any injury to people or property resulting from any ideas, methods, instructions or products referred to in the content.